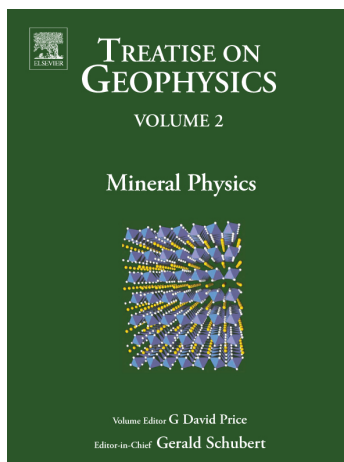


**Provided for non-commercial research and educational use.
Not for reproduction, distribution or commercial use.**

This article was originally published in the Treatise on Geophysics, published by Elsevier and the attached copy is provided by Elsevier for the author's benefit and for the benefit of the author's institution, for non-commercial research and educational use including use in instruction at your institution, posting on a secure network (not accessible to the public) within your institution,



and providing a copy to your institution's administrator.

All other uses, reproduction and distribution, including without limitation commercial reprints, selling or licensing copies or access, or posting on open internet sites are prohibited. For exceptions, permission may be sought for such use through Elsevier's permissions site at:

<http://www.elsevier.com/locate/permissionusematerial>

Information taken from the copyright line. The Editor-in-Chief is listed as Gerald Schubert and the imprint is Academic Press.

2.05 Mineralogy of the Earth – The Earth’s Core: Iron and Iron Alloys

L. Vočadlo, University College London, London, UK

© 2007 Elsevier B.V. All rights reserved.

2.05.1	Introduction	91
2.05.2	Seismological Observations of the Earth’s Core	92
2.05.2.1	PREM and Beyond	92
2.05.2.2	Anisotropy and Layering in the Inner Core	92
2.05.2.3	Super-Rotation of the Inner Core	94
2.05.2.4	Seismological Observations of the Outer Core	95
2.05.3	The Structure of Iron in the Inner Core	95
2.05.4	Thermoelastic Properties of Solid Iron	98
2.05.4.1	Thermodynamic Properties from Free Energies	98
2.05.4.1.1	Equation of state	99
2.05.4.1.2	Incompressibility	99
2.05.4.1.3	Thermal expansion	99
2.05.4.1.4	Heat capacity	99
2.05.4.1.5	Grüneisen parameter	100
2.05.4.2	Elasticity of Solid Iron	101
2.05.5	Rheology of Solid Iron	102
2.05.5.1	Slip Systems in Iron	102
2.05.5.2	Viscosity and the Inner Core	104
2.05.6	The Temperature in the Earth’s Core	106
2.05.7	Thermodynamic Properties of Liquid Iron	108
2.05.8	Rheology of Liquid Iron	108
2.05.8.1	Viscosity and Diffusion	108
2.05.8.2	The Structure of Liquid Iron	110
2.05.9	Evolution of the Core	110
2.05.10	The Composition of the Core	111
2.05.10.1	Bulk Composition	111
2.05.10.2	The Effect of Nickel	112
2.05.10.3	Light Elements	112
2.05.10.3.1	Chemical potential calculations of FeX binary systems	112
2.05.10.3.2	High-temperature elasticity of FeSi and FeS	114
2.05.10.3.3	Rheology of liquid iron alloys	116
2.05.11	Summary	116
References		117

2.05.1 Introduction

The Earth’s core plays a fundamental role in the evolution of our planet. As the Earth cools, the inner core grows, crystallizing from the outer core of liquid iron (alloyed with \sim 5–10% light elements) to form an inner core of solid iron (alloyed with \sim 2–3% light elements (Jephcoat and Olson, 1987; Poirier, 1994; Stixrude *et al.*, 1997; Alfè *et al.*, 2002a)). The release of latent heat of

fusion, together with chemical buoyancy arising from the enrichment of the outer core with light elements, provide driving forces for the fluid flow responsible for the geodynamo, and hence for the Earth’s magnetic field. The heat released from the core helps drive mantle convection which leads in turn to surface features such as volcanism and plate tectonics. Since the inner core is sitting within the liquid outer core, it is isolated from the rest of the Earth; however, coupling

with the outer core and mantle (e.g., geomagnetic and gravitational) prevent its motion from being entirely independent, allowing it to super-rotate and wobble.

The only direct observations of the Earth's core come from seismology; therefore, any credible mineralogical model has to match exactly the seismic observations. Increasingly accurate seismic observations have shown the Earth's inner core, in particular, to be far more complex than had previously been thought. The current seismological models reveal an inner core which is anisotropic, layered, and possibly laterally heterogeneous, but the origins of this anisotropy and layering are not yet understood. It is generally considered that the anisotropy reflects the preferred orientation of the crystals present, which could have arisen either during inner-core crystallization or developed over time through solid state flow; these two mechanisms have vastly different implications for core evolution. The observed layering may be due to changes in chemical composition, crystal structure, preferred orientation or some combination of all three. Again, these imply very different core processes and evolution. The observed layering also implies that the upper and lower inner core could be compositionally or structurally different. The origin of anisotropy and layering is fundamental to understanding and constraining evolutionary models for the Earth's inner core, and the mineralogical model must reflect this complex structure.

Mineral physics also has an important role to play in understanding the processes going on in the outer core. Knowledge of the thermoelastic properties of candidate liquid iron alloys can be compared with seismological observations and therefore lead to models for the composition of the outer core. Estimates for the dynamic properties of liquids such as diffusivity and viscosity can be incorporated into the magnetohydrodynamics equations that quantify the magnetic field (*see Chapter 5.03*). Furthermore, mineral physics can provide values for thermodynamic quantities that can be put into thermal evolution models of core formation leading to time-scales for inner core growth and quantification of the heat budget of the Earth.

In order to place fundamental constraints on the properties of the Earth's core, it is essential to know the behavior of iron and iron alloys at core conditions. In particular, the key questions to resolve are: what is the most stable phase(s) of iron present in the inner core, what are the elastic properties of the stable phase(s) (at core pressures and temperatures), what are the rheological properties of these candidate solid phases, do the combined thermoelastic and rheological properties of iron alloys lead to a comprehensive model for inner

core composition, evolution, anisotropy, and layering; in addition, what is the temperature of the Earth's core, what are the thermodynamic properties of candidate liquid iron alloy phases, what are the rheological properties of these phases, what is the composition of the outer core. Notwithstanding the difficulties in answering any single one of these questions, the combined answers of them all should exactly match the models inferred from seismology.

2.05.2 Seismological Observations of the Earth's Core

2.05.2.1 PREM and Beyond

One-dimensional global seismological models for the Earth's core, such as the 'preliminary reference Earth model' (PREM; Dziewonski and Anderson, 1981), give bulk elastic properties as a function of depth via compressional and shear wave velocity profiles and free oscillation data. Although these models tell us nothing about exact composition or temperature, they do give fairly robust measurements for pressure, density, and also elastic moduli, such as incompressibility and shear modulus, from which compositional models can be derived. Since PREM there have been a number of refinements of the seismological model such as IASP91 (Kennett and Engdahl 1991) and AK135 (Kennett *et al.*, 1995) which show subtle differences in the detailed velocity profiles, but are generally consistent with each other. More complex structures of the Earth have been observed with three-dimensional (3-D) imaging generated using seismic tomography; this shows how the wave velocities vary laterally as well as radially generating a 3-D representation of wave velocities throughout the Earth (see, e.g., Romanowicz (2003) for a review). It is the job of mineral physics to provide estimates for core properties which best match these seismological models and which thereby provide an explanation for the more detailed seismic structure of the inner core.

2.05.2.2 Anisotropy and Layering in the Inner Core

It is well established that the inner core exhibits significant anisotropy, with P-wave velocities $\sim 3\%$ faster along the polar axis than in the equatorial plane (Creager, 1992; Song and Helmberger, 1993; Song, 1997; Song and Xu, 2002; Sun and Song, 2002; Beghein and Trampert, 2003; Oreshin and Vinnik, 2004). Early models for the inner core suggested that this seismic

anisotropy had cylindrical symmetry, with the symmetry axis parallel to the Earth's rotation axis. More recent seismic observations suggest that, as well as being cylindrically anisotropic, the inner core may in fact be layered (**Figure 1(a)**). The evidence is for a seismically isotropic or weakly anisotropic upper layer, with lateral variations in thickness of $\sim 100\text{--}400$ km, overlaying an irregular, nonspherical transition region to an anisotropic lower layer (Song and Helmberger, 1998; Ouzounis and Creager, 2001; Song and Xu, 2002; Ishii and Dziewonski, 2003), although variations on this model have also been suggested (e.g., **Figure 1(b)**). The existence of an isotropic upper layer implies that the magnitude of the seismic anisotropy in the lower inner core should be significantly greater than previously thought, possibly as much as 5–10% (Ouzounis and Creager, 2001; Song and Xu, 2002). The observed layering also implies that the upper and lower inner core could be compositionally or structurally different.

With this recently observed complex structure of the inner core, the question arises as to the mechanisms by which such anisotropy and layering can occur, and the nature of the seismic boundary. The isotropic layer could be due either to randomly oriented crystals (containing, e.g., b.c.c. and/or h.c.p. iron) or to a material with a low intrinsic anisotropy. The anisotropic lower layer is thought to be due to the preferred orientation of aligned crystals (Anderson, 1989), possibly, although not

necessarily, of a different iron phase to the upper layer. The inner core could therefore, for example, be comprised entirely of b.c.c. iron, entirely of h.c.p. iron, or some combination of the two.

There are three hypotheses of how the anisotropy and layering could have occurred:

1. Yoshida *et al.* (1996) have suggested a driving mechanism whereby the inner core grows more rapidly at the equator than the poles, giving rise to a flattened sphere. In order to maintain hydrostatic equilibrium, this ellipsoidal inner core would have to continuously deform as it grows, resulting in stress-induced recrystallization. **Figure 2** shows the flow lines resulting from their calculations. In this model, the older material will have undergone the most deformation, and hence show the greatest preferential orientation, consistent with the observation that the center of the inner core has a greater degree of anisotropy.

2. Buffett and Wenk (2001) suggested instead that the depth dependence of anisotropy can be explained by plastic deformation under the influence of electromagnetic shear stresses (**Figure 3**). This would produce a toroidal type flow, quite different from that of the previous model. Again, the high anisotropy in the lower inner core results from the fact that it is older and has had more time to develop.

3. The third possibility is that the preferred orientation was locked into the crystal on cooling from the

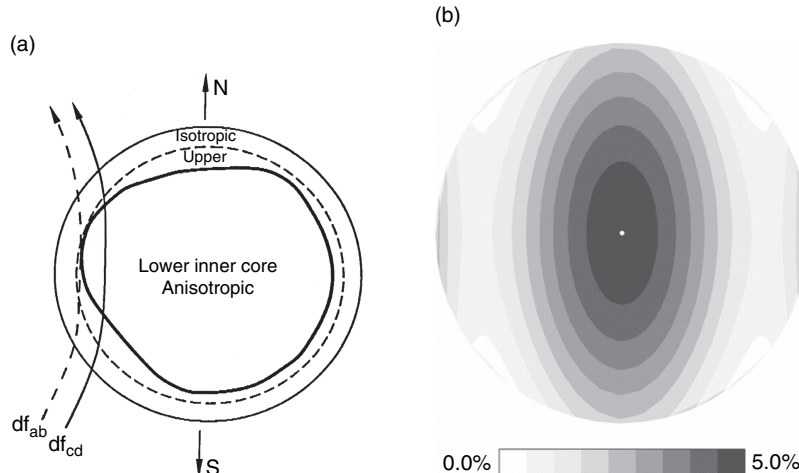


Figure 1 (a) Schematic of isotropic upper-inner-core and anisotropic lower-inner-core structure. The boundary is speculated to be irregular, which may explain recent reports of large scatter in inner core travel times. (b) Cross section through the axisymmetric anisotropic inner-core model. The contour levels show the compressional-velocity perturbations relative to PREM for waves traveling parallel to the rotation axis. Note that this inner-core model is highly anisotropic near its center. The ability of the model to fit the inner-core spectral data degrades appreciably if an isotropic layer thicker than 100–200 km is imposed at the top of the inner core. (a): Song XD and Helmberger DV (1998) Seismic evidence for an inner core transition zone. *Science* 282: 924–927; (b): Durek JJ and Romanowicz B (1999) Inner core anisotropy by direct inversion of normal mode spectra. *Geophysical Journal International* 139: 599–622.

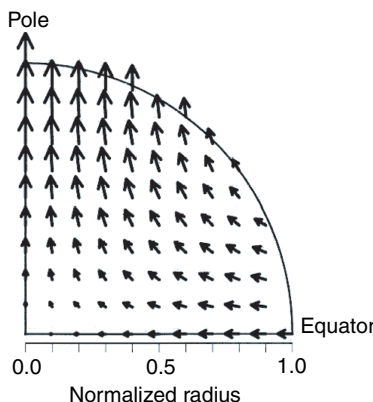


Figure 2 Flow field showing predominantly radial flow. From Yoshida S, Sumita I, and Kumazawa M (1996) Growth model of the inner core coupled with outer core dynamics and the resulting anisotropy. *Journal of Geophysical Research* 101: 28085–28103.

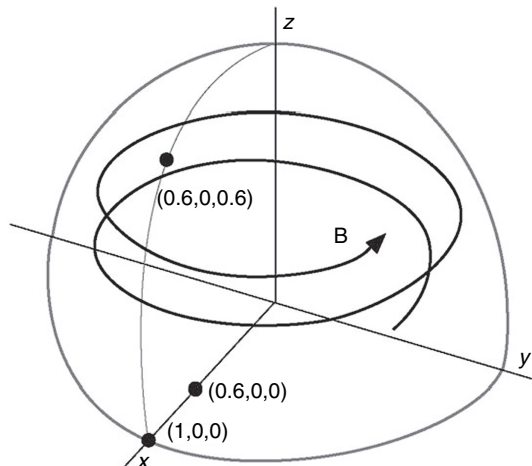


Figure 3 Direction of magnetic field causing preferred crystal alignment in model of Buffett and Wenk (2001).

liquid, perhaps due to flow in the outer core (Karato, 1993). If the alignment was frozen in on crystallization, there would have to be an, as yet unknown, mechanism for the formation of the outer isotropic layer. One possibility is simply that the iron phase in the outer layer of the inner core is different to that in the deeper inner core and does not have slip systems which cause anisotropy.

The first model predicts the *c*-axis of h.c.p.-iron to be aligned parallel to the pole directions, while the second mode predicts it to be in the equatorial plane. Despite the completely different underlying dynamics and resultant flow fields, both studies were able to show at the time of publication (1996 and 2001, respectively) that the predicted lattice

preferred orientation gave an anisotropy consistent with that observed for the inner core. The reason they were able to do this was because they used different sets of elastic constants to calculate the anisotropy (see Section 2.05.4.2), and they used different mechanisms for producing the preferred orientation in the first place. An additional, but fundamental uncertainty in these models is that they only considered the h.c.p. phase of iron. As shown in Section 2.05.3, there is growing evidence that b.c.c. may in fact be stable in all or part of the inner core.

2.05.2.3 Super-Rotation of the Inner Core

In addition to anisotropy and layering, there is another inference from seismology which provides a constraint on the dynamics of the inner core, in particular, inner-core viscosity. Seismic observations suggest that the Earth's inner core may be rotating with respect to the bulk of the Earth. Although there have been several seismic studies, until recently, there appeared to be no consensus as to the amount of differential rotation of the Earth's core with respect to the mantle. Observations suggest rotation rates which range from marginally detectable to 3° per year (Song and Richards, 1996; Su *et al.*, 1996; Creager, 1997; Song, 2000; Song and Li, 2000; Souriau, 1998; Poupinet *et al.*, 2000; Collier and Helffrich, 2001). More recently, however, the debate seems to have settled on the low end of the spectrum at $0.3\text{--}0.5^\circ$ per year (Zhang *et al.*, 2005). If the rotation rate is high, and if seismic anisotropy is due to preferred alignment, the inner core would have to adjust on a relatively short timescale in order to maintain its texture as it rotates. Collier and Helffrich (2001) suggested that the relative motion of the inner core and the mantle might take the form of an inner-core oscillation on a timescale of ~ 280 days rather than a simple relative rotation of the two; this type of oscillation could be caused by the heterogeneous distribution of mass in the Earth's mantle exerting a significant gravitational pull on the inner core, which will tend to keep the inner core aligned. The extent to which the inner core adjusts during differential rotation or oscillation will therefore depend critically on the inner-core viscosity. Buffett (1997) modeled the viscous relaxation of the inner core by calculating numerically the relaxation time for the inner core to adjust, as it rotates, back to its equilibrium shape after small distortions due to perturbations in gravitational potential imposed by the overlying mantle. He suggested that the viscosity has to be constrained to be either less than 10^{16} Pa s or greater than 10^{20} Pa s depending on the

dynamical regime. The latter value is supported by Collier and Hellfrich (2001), who concluded that the attenuation of the observed inner-core torsional oscillations with time are consistent with a viscosity of 3.9×10^{19} Pa s. Clearly, an independent measure of inner-core viscosity would place constraints on these values which will depend not only on the crystal structure adopted by the iron alloy of the inner core but also on the mechanism(s) by which deformation occurs.

2.05.2.4 Seismological Observations of the Outer Core

In general, the outer core is considered to be homogeneous due to the continual mixing of the liquid via convection. Despite this, there is some seismological evidence to suggest that there is some structure and heterogeneity in the outer core. For example, lateral velocity heterogeneities, possibly associated with the topography at the core–mantle boundary (CMB), have been observed with seismic tomography (Soldati *et al.*, 2003). However, at the present time, it is impossible to be definitive as to whether or not these lateral anomalies are an artifact of the methodology (see, e.g., Lei and Zhao, 2006). There is also some evidence for some structure at the top of the outer core. A very small (a few kilometers across) and thin (150 m) outer core rigidity zone may exist just below the core–mantle boundary (Garnero and Jeanloz, 2000); it is possible that this anomaly is responsible for the wobbling of the Earth's rotation axis (Rost and Revenaugh, 2001). Finally, there may be a mushy layer (crystals suspended in liquid) or slurry zone (solidification via dendrites) at the base of the inner core, the latter being more likely (Shimizu *et al.*, 2005).

Accurate mineral physics data can be used to resolve many of the uncertainties about the structure and composition of the Earth's core; however, as mentioned in Section 2.05.1, the mineralogical model that comes out of combining theoretical and experimental studies must match the seismological observations exactly. Furthermore, the seismological observations themselves must be sufficiently detailed and robust to enable accurate and meaningful comparisons to be made.

2.05.3 The Structure of Iron in the Inner Core

The properties of the inner core are determined by the materials present; although we know that the inner

core is made of iron alloyed with nickel and other lighter elements (see Section 2.05.10), we must first understand the behavior of pure iron before we are able to understand the behavior of iron alloys. However, the properties of pure iron relevant to the Earth's core depend upon the structure iron adopts at core conditions, and it is this we need to address first.

Experimentalists have put an enormous effort over the last 15–20 years into obtaining a phase diagram of pure iron, but above relatively modest pressures and temperatures there is still much uncertainty (Brown, 2001). Under ambient conditions, Fe adopts a b.c.c. structure, that transforms with temperature to an f.c.c. form, and with pressure transforms to an h.c.p. phase, ε -Fe. The high P/T phase diagram of pure iron itself however is still controversial (see Figure 4 and also the discussion in Stixrude and Brown (1998)). Various diamond anvil cell (DAC)-based studies have been interpreted as showing that h.c.p. Fe transforms at high temperatures to a phase which has variously been described as having a double hexagonal close packed structure (dh.c.p.) (Saxena *et al.*, 1996) or an orthorhombically distorted h.c.p. structure (Andrault *et al.*, 1997). Furthermore, high-pressure shock experiments have also been interpreted as showing a high-pressure solid–solid phase transformation (Brown and McQueen, 1986; Brown, 2001), which has been suggested could be due to the development of a b.c.c. phase (Matsui and Anderson, 1997). Other experimentalists, however, have failed to detect such a post-h.c.p. phase (e.g., Shen *et al.*, 1998; Nguyen and Holmes, 2004), and have suggested that the previous observations were due to either minor impurities or metastable strain-induced behavior. Nevertheless, the experiments, together with theoretical calculations of the static, zero-Kelvin solid (Stixrude *et al.*, 1997; Vočadlo *et al.*, 2000), suggested that the h.c.p. phase of iron is the most likely stable phase in the inner core. Experiments at moderate pressure and ambient temperature (Antonangeli *et al.*, 2004), and calculations (Stixrude and Cohen, 1995a) at high pressures but at 0 K, showed that the compressional wave velocity along the c -axis of h.c.p.-Fe is significantly faster than that in the basal plane; this led to the conclusion that the inner core is made up of oriented h.c.p.-Fe crystals with the c -axis parallel to the rotation axis. However, more recent calculations (using a particle-in-cell (PIC) method) found that the elastic properties of h.c.p.-Fe change dramatically as a function of temperature (Steinle-Neumann *et al.*, 2001), and that compressional waves travel faster in the basal plane of h.c.p.-Fe at high temperatures and pressures, in

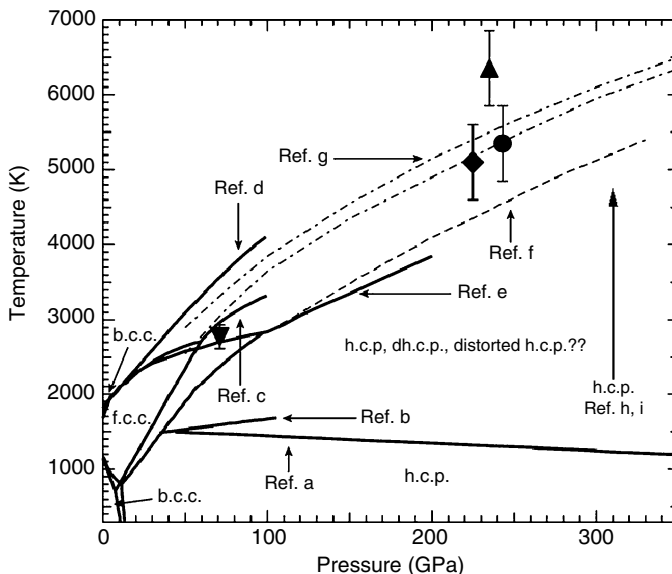


Figure 4 Phase diagram of pure iron. Solid lines represent phase boundaries and melt lines from DAC experiments; symbols with error bars are points on the melting curve from shock experiments; broken lines are melting curves from first-principles calculations. DAC data: Ref. a: Saxena and Dubrovinsky (2000); b: Andrault *et al.* (2000); c: Shen *et al.* (1998); d: Williams *et al.* (1987); e: Boehler (1993). Shock data: triangle: Yoo *et al.* (1993); circles: Brown and McQueen (1986); reverse triangle: Ahrens *et al.* (2002); diamond: Nguyen and Holmes (2004). First principles calculations; f: Lai *et al.* (2000); g: Alfè *et al.* (2002a, 2002b); h: Vočadlo *et al.* (2000); i: Vočadlo *et al.* (2003a, 2003b). Adapted from Nguyen JH and Holmes NC (2004) Melting of iron at the physical conditions of the Earth core. *Nature* 427: 339–342.

complete contrast to the low-temperature results. These results can account for the observed seismic anisotropy if the preferred orientation of h.c.p.-Fe in the inner core is with the α -axis aligned parallel to the equatorial plane instead of parallel to the poles. Obviously, if the seismic anisotropy is caused by deformation, the two studies imply very different stresses and flow fields in the inner core (as described in Section 2.05.2.2). There are two main issues with these conclusions that need to be considered.

First, the assumption that iron must have the h.c.p. structure at core conditions has been recently challenged, especially in the presence of lighter elements (Beghein and Trampert, 2003 and Figure 5; Lin *et al.*, 2002) – it now seems possible or even probable that a b.c.c. phase might be formed (Vočadlo *et al.*, 2003a).

Previously, the b.c.c. phase of iron was considered an unlikely candidate for a core-forming phase because it is elastically unstable at high pressures, with an enthalpy considerably higher than that of h.c.p. (Söderlind *et al.*, 1996; Stixrude and Cohen, 1995b; Vočadlo *et al.*, 2000). However, *ab initio* molecular dynamics calculations to obtain free energies at core pressures and temperatures have found that the b.c.c. phase of iron does, in fact, become entropically

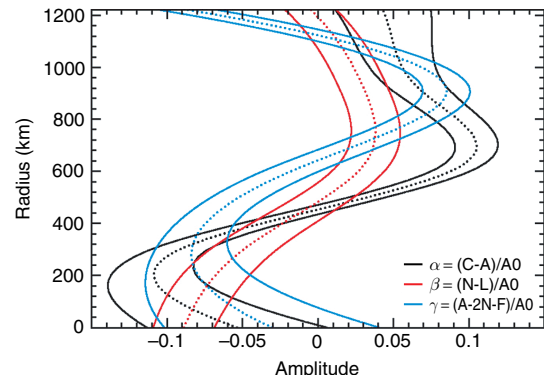


Figure 5 Anisotropy models taken from Beghein and Trampert (2003). The thin dotted line represents the mean model, and the thick surrounding lines correspond to two standard deviations. α , β , and γ are the three anisotropic parameters describing P-wave anisotropy, S-wave anisotropy, and the anisotropy of waves that do not travel along the vertical or horizontal directions, respectively. A comparison with the elasticity of h.c.p. iron at inner-core conditions (Steinle-Neumann *et al.*, 2001) shows that some of their models can be explained by progressively tilted h.c.p. iron in the upper half of the inner core, with their symmetry axes oriented at 45° from Earth's rotation axis at $r = 900$ km and at 90° in the middle of the inner core. In the deepest inner core ($r = 0$ –400 km), ‘none’ of their models is compatible with published data of h.c.p. iron. This result might suggest the presence of another phase from these depths. Such a phase of iron could indeed be stable in the presence of impurities.

stabilized at core temperatures (Vočadlo *et al.*, 2003a). In an earlier paper (Vočadlo *et al.*, 2000) spin-polarized simulations were initially performed on candidate phases (including a variety of distorted b.c.c. and h.c.p. structures and the dh.c.p. phase) at pressures ranging from 325 to 360 GPa. These revealed, in agreement with Söderlind *et al.* (1996), that under these conditions only b.c.c. Fe has a residual magnetic moment and all other phases have zero magnetic moments. It should be noted, however, that the magnetic moment of b.c.c. Fe disappears when simulations are performed at core pressures and an electronic temperature of >1000 K, indicating that even b.c.c. Fe will have no magnetic stabilization energy under core conditions. At these pressures, both the b.c.c. and the suggested orthorhombic polymorph of iron (Andrault *et al.*, 1997) are mechanically unstable (**Figure 6**). The b.c.c. phase can be continuously transformed to the f.c.c. phase (confirming the findings of Stixrude and Cohen (1995a)), while the orthorhombic phase spontaneously transforms to the h.c.p. phase, when allowed to relax to a state of isotropic stress.

In contrast, h.c.p., dh.c.p., and f.c.c. Fe remain mechanically stable at core pressures, and we were therefore able to calculate their phonon frequencies and free energies. These showed that the h.c.p. phase was the more stable phase. However, it must be remembered that the free energies were obtained from phonon frequencies calculated at 0 K. More recently, Vočadlo *et al.* (2003a) used the method of thermodynamics integration combined with *ab initio* molecular dynamics to calculate the free energy at core pressures and temperatures of b.c.c. and h.c.p. iron. The conclusion was that, although the thermodynamically most stable phase of pure iron is still the h.c.p. phase, the free energy difference is so very small (**Table 1**) that a small amount of light element impurity could stabilize the b.c.c. phase at the expense of the h.c.p. phase (Vočadlo *et al.*, 2003a).

Second, considerable doubts have now been cast over the PIC method used to calculate the high-temperature elastic constants (Gannarelli *et al.*, 2003). Of particular importance is use of the correct

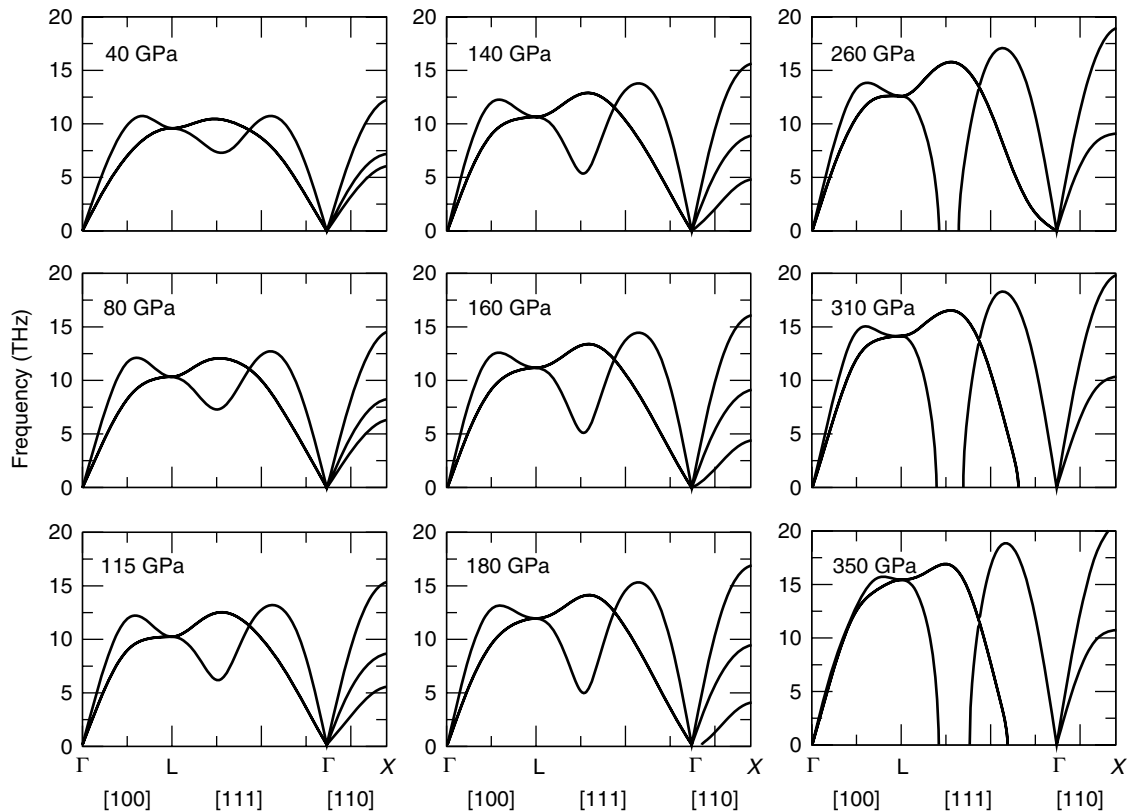


Figure 6 The calculated phonon dispersion curves for b.c.c.-Fe at nine different volumes (corresponding to $\sim 40\text{--}350$ GPa) (Vočadlo *et al.*, 2003a). The softening in the [110] direction at ~ 180 GPa indicates the onset of the b.c.c. \rightarrow f.c.c. transition, and that in the [111] direction above ~ 260 GPa corresponds to the b.c.c. $\rightarrow \omega$ transition.

Table 1 The *ab initio* Helmholtz free energy per atom of the b.c.c. and h.c.p. phases of Fe at state points along (*) and below) the calculated melting curve

V (Å ³)	T (K)	F _{bcc} (eV)	F _{hcp} (eV)	ΔF (meV)
9.0	3500	-10.063	-10.109	46
8.5	3500	-9.738	-9.796	58
7.8	5000	-10.512	-10.562	50
7.2	6000	-10.633	-10.668	35
6.9	6500	-10.545	-10.582	37
6.7	6700	-10.288	-10.321	33
7.2*	3000	-7.757	-7.932	175

Vočadlo L, Alfe D, Gillan MJ, Wood IG, Brodholt JP, and Price GD (2003a) Possible thermal and chemical stabilisation of body-centred-cubic iron in the Earth's core. *Nature* 424: 536–539. Note that at core conditions, ΔF is only ~35 meV.

equilibrium c/a ratio in h.c.p.-Fe; indeed, there has been an evolving story in the literature just on this property of iron alone, as it has a significant effect on the nature of the elastic anisotropy. In their work on the high-pressure, high-temperature elastic properties of h.c.p.-Fe, Steinle-Neumann *et al.* (2001) reported an unexpectedly large c/a ratio of almost 1.7. However, the work of Gannarelli *et al.* (2005) casts doubt on the robustness of these calculations and they found that the c/a ratio ranges from 1.585 at zero pressure and temperature to 1.62 at 5500 K and 360 GPa (see Figure 7), a result confirmed by further calculations (Vočadlo, 2007).

It should be clear from this section that neither the stable phase(s) nor the elasticity of iron in the Earth's inner core are known with any certainty; the studies outlined above serve to highlight the need to perform more detailed calculations under the appropriate conditions of pressure and temperature. Although the free energy of h.c.p.-Fe is lower than that of b.c.c.-Fe, even for a hypothetical pure iron core, the free energy difference is so small that, at core temperatures, both phases are likely to exist. In addition, we need to consider the effect of light elements, not only on the stability of the phases, but also on seismic anisotropy and slip systems.

2.05.4 Thermoelastic Properties of Solid Iron

The only experimental data on solid iron under true core pressures and temperatures comes from either simultaneously high- P /high- T static experiments or shock experiments; however, although the

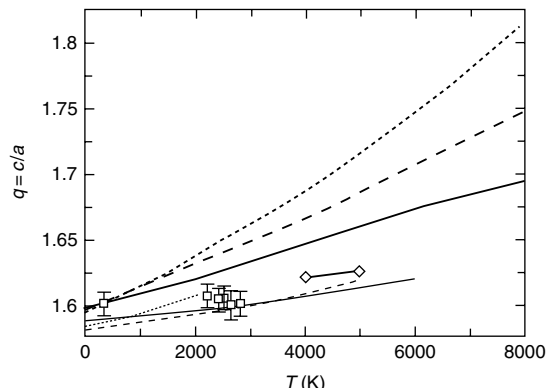


Figure 7 Calculated equilibrium axial ratio as a function of temperature for different volumes (light curves). Atomic volumes are 6.97 Å³ (solid curve), 7.50 Å³ (dashed curve), and 8.67 Å³ (dotted curve). For Steinle-Neumann *et al.* (2001) (heavy curves) volumes are 6.81 Å³ (solid curve), 7.11 Å³ (dashed curve), and 7.41 Å³ (dotted curve). Also shown are diffraction measurements due to Ma *et al.* (2004) at 7.73 Å³/atom (open squares with error bars) and *ab initio* MD calculations (open diamonds) at 6.97 Å³ (Gannarelli *et al.*, 2005). After Gannarelli CMS, Alfé D, and Gillan MJ (2005) The axial ration of hcp iron at the conditions of the Earth's inner core. *Physics of the Earth and Planetary Interiors* 139: 243–253.

measurement of temperature in shock experiments has been attempted, it is problematic (e.g. Yoo *et al.*, 1993). There are a number of static experimental studies on pure iron at ambient pressures and high temperatures, and high pressures and ambient temperatures (see below). Simultaneously high-pressure/high-temperature experiments are very challenging, although they have been attempted (e.g., the iron phase diagram above). In this section, we look at the thermoelastic properties of iron as obtained from *ab initio* calculations, and, where possible, compare them to experimental data.

2.05.4.1 Thermodynamic Properties from Free Energies

Computational mineral physics can play an extremely important role in quantifying some of the key thermodynamics properties that determine the state and evolution of the inner core. These calculations both compliment experimental data, and extend our knowledge where no experimental data exist. In Section 2.05.3 we have already shown that 'pure' iron is likely to take the h.c.p. structure at core conditions, so for the properties we present here, we focus only on h.c.p.-Fe. The results are presented as a function of pressure along isotherms. At each

temperature, the results are only shown for the pressure range where, according to the calculations, the h.c.p. phase is thermodynamically stable. The calculated thermodynamic properties at a given temperature, T , and pressure, P , can be determined from the Gibbs free energy, $G(P, T)$. In practice, we calculate the Helmholtz free energy, $F(V, T)$, as a function of volume, V , and hence obtain the pressure through the relation $P = -(\partial F / \partial V)T$ and G through its definition $G = F + PV$. To calculate the free energies we use the method of thermodynamic integration which allows us to calculate the difference in free energy, $F - F_0$, between our *ab initio* system and a reference system whose potential energies are U and U_0 respectively. Technical details of the methodology can be found in Alfè *et al.* (2001).

2.05.4.1.1 Equation of state

The equation of state for h.c.p.-Fe has been studied both experimentally (e.g., Mao *et al.*, 1990; Brown and McQueen, 1986) and theoretically (e.g., Söderlind *et al.*, 1996). In **Figure 8** we show the density as a function of pressure from *ab initio* calculations together with that from static compression measurements at 300 K (Mao *et al.*, 1990), shock experiments (Brown and McQueen, 1986), theoretical calculations (Stixrude

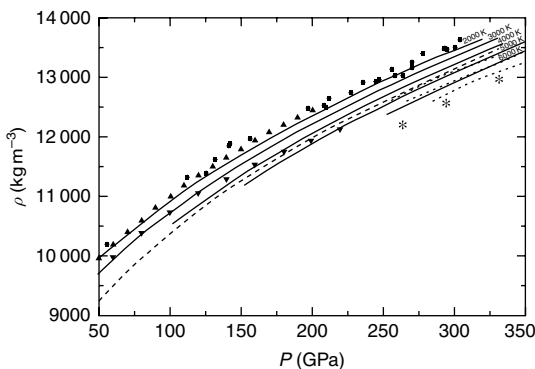


Figure 8 Density as a function of pressure for h.c.p. iron from *ab initio* calculations along isotherms between 2000 and 6000 K. Filled circles are the static compression measurements at 300 K (Mao *et al.*, 1990); dashed line is the calculations for the 4000 K isotherm of Stixrude *et al.* (1997); dotted lines are the 5000 K, 6000 K, and 7000 K isotherms of Steinle-Neumann *et al.*, (2002); stars are from an analysis of a thermal equation of state at 6000 K (Isaak and Anderson, 2003); triangles-up and -down are the experiments of Brown and McQueen (1986) along the 300 K isotherm and Hugoniot respectively. Modified from Vočadlo L, Alfè D, Gillan MJ, and Price GD (2003b) The properties of iron under core conditions from first principles calculations. *Physics of the Earth and Planetary Interiors* 140: 101–125.

et al., 1997; Steinle-Neumann *et al.*, 2002) and an analysis at 6000 K based on a thermal equation of state (Isaak and Anderson, 2003). All the results from both theory and experiment are in comforting agreement and provide a successful basis from which to make further comparisons of other properties.

2.05.4.1.2 Incompressibility

The isothermal and adiabatic incompressibility (K_T and K_S , respectively) are shown in **Figure 9**. The incompressibility increases significantly (and almost linearly) with pressure, and decreases with increasing temperature (more so in the case of K_T than K_S).

2.05.4.1.3 Thermal expansion

The thermal expansivity, α , is shown in **Figure 10** together with the value determined from shock data at 5200 K (Duffy and Ahrens, 1993), the theoretical calculations of Stixrude *et al.* (1997), and an analysis using a thermal equation of state (Anderson and Isaak, 2002; Isaak and Anderson, 2003). It is clear that α decreases strongly with increasing pressure and increases significantly with temperature.

2.05.4.1.4 Heat capacity

The total constant-volume specific heat per atom C_v (**Figure 11**) emphasizes the importance of electronic excitations in our calculations. In a purely harmonic system, C_v would be equal to $3k_B$, and it is striking that C_v is considerably greater than that even at

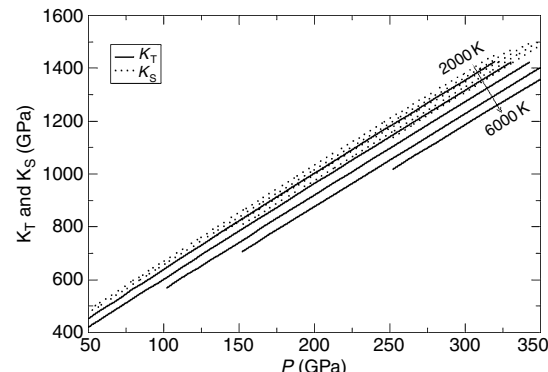


Figure 9 Isothermal incompressibility, K_T (solid lines), and adiabatic incompressibility, K_S (dotted lines), as a function of pressure for h.c.p. iron from *ab initio* calculations along isotherms between 2000 and 6000 K. From Vočadlo L, Alfè D, Gillan MJ, and Price GD (2003b) The properties of iron under core conditions from first principles calculations. *Physics of the Earth and Planetary Interiors* 140: 101–125.

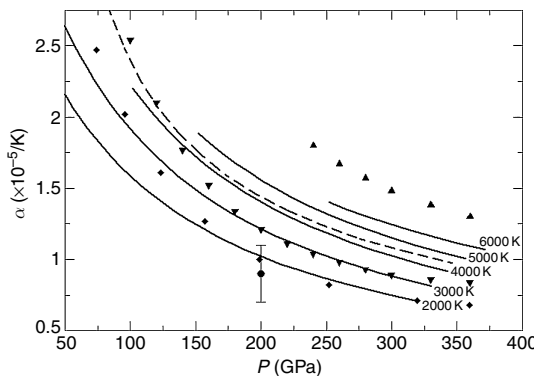


Figure 10 Thermal expansion as a function of pressure for h.c.p. iron from *ab initio* calculations along isotherms between 2000 and 6000 K (solid lines). The circle is the value of Duffy and Ahrens (1993) determined from shock experiments at 5200 ± 500 K; the dashed line is from theoretical calculations for the 4000 K isotherm (Stixrude *et al.*, 1997); the diamonds are from an analysis of room temperature compression data at 300 K (Anderson and Isaak, 2002); the triangles (up: 6000 K, down: 2000 K) are from an analysis using a thermal equation of state applied to room temperature compression data (Isaak and Anderson, 2003). Modified from Vočadlo L, Alfe D, Gillan MJ, and Price GD (2003b) The properties of iron under core conditions from first principles calculations. *Physics of the Earth and Planetary Interiors* 140: 101–125.

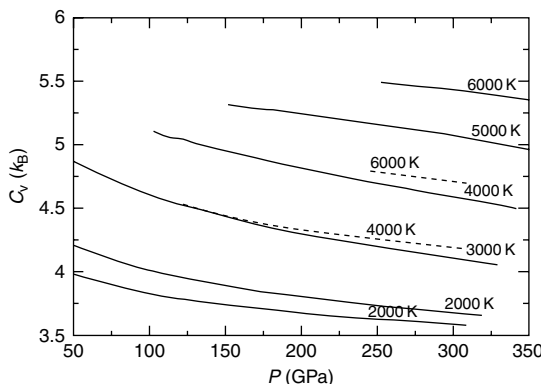


Figure 11 Constant volume heat capacity as a function of pressure for h.c.p. iron from *ab initio* calculations along isotherms between 2000 and 6000 K (solid lines). The much lower dashed lines are from Stixrude *et al.* (1997). Modified from Vočadlo L, Alfe D, Gillan MJ, and Price GD (2003b) The properties of iron under core conditions from first principles calculations. *Physics of the Earth and Planetary Interiors* 140: 101–125.

the modest temperature of 2000 K, while at 6000 K it is nearly doubled. The decrease of C_v with increasing pressure evident in Figure 9 comes from the suppression of electronic excitations by high compression, and to a smaller extent from the

suppression of anharmonicity. Our C_v values are significantly higher than those of Stixrude *et al.* (1997); this is likely to be due to the inclusion of anharmonic corrections via *ab initio* molecular dynamics and the temperature dependence of harmonic frequencies.

2.05.4.1.5 Grüneisen parameter

The Grüneisen parameter, γ , is an important quantity in geophysics as it often occurs in equations which describe the thermoelastic behavior of materials at high pressures and temperatures. The value for γ is used to place constraints on geophysically important parameters such as the pressure and temperature dependence of the thermal properties of core, the adiabatic temperature gradient, and the geophysical interpretation of Hugoniot data. The Grüneisen parameter has considerable appeal to geophysicists because it is an approximately constant, dimensionless parameter that varies slowly as a function of pressure and temperature. It has both a microscopic and macroscopic definition, the former relating it to the vibrational frequencies of atoms in a material, and the latter relating it to familiar thermodynamic properties such as heat capacity and thermal expansion. Unfortunately, the experimental determination of γ , defined in either way, is extremely difficult; the microscopic definition requires a detailed knowledge of the phonon dispersion spectrum of a material, whereas the macroscopic definition requires experimental measurements of thermodynamic properties at simultaneously high pressures and temperatures.

The microscopic definition of the Grüneisen parameter (Grüneisen, 1912) is written in terms of the volume dependence of the i th mode of vibration of the lattice (ω_i) and is given by

$$\gamma_i = -\frac{\partial \ln \omega_i}{\partial \ln V} \quad [1]$$

However, evaluation of all γ_i throughout the Brillouin zone is impossible without some lattice dynamical model or high pressure inelastic neutron scattering data. It can be shown (e.g., Barron, 1957) that the sum of all γ_i throughout the first Brillouin zone leads to a macroscopic or thermodynamic definition of g which may be written as

$$\gamma_{tb} = \frac{\alpha V K_T}{C_v} \quad [2]$$

where α is the thermal expansion, V is the volume, K_T is the isothermal bulk modulus, and C_v is the heat capacity at constant volume. Evaluation of γ_i is also very difficult, however, because it requires experimental measurements of α , K_T , etc., at extreme conditions of pressure and temperature which are not readily attainable. Integrating the above equation with respect to temperature at constant volume leads to the Mie-Grüneisen expression for γ (see, e.g., Poirier 2000):

$$\gamma_{\text{th}} = \frac{P_{\text{th}} V}{E_{\text{th}}} \quad [3]$$

where P_{th} is the thermal pressure and E_{th} is the thermal energy. This too is difficult to determine because the thermal energy is not readily obtained experimentally. At low temperatures, where only harmonic phonons contribute to E_{th} and P_{th} , γ should indeed be temperature independent above the Debye temperature, because $E_{\text{th}}=3k_B T$ per atom, and $P_{\text{th}}V=-3k_B T(d \ln \omega/d \ln V)=3k_B T\gamma_{\text{ph}}$, so that $\gamma_{\text{th}}=\gamma_i$ (the phonon Grüneisen parameter above). But in iron at high temperatures, the temperature independence of γ will clearly fail, because of electronic excitations and anharmonicity. Our results for γ (Figure 12) indicate that it varies rather little with either pressure or temperature in the region of interest. At temperatures below ~ 5000 K, it decreases with increasing pressure, as expected from the behavior of γ_i . This is also expected from the often-used empirical rule of thumb $\gamma=(V/V_0)^q$, where V_0 is a reference volume and q is a constant exponent usually taken to be roughly unity. Since V decreases by a factor of about 0.82 as P goes

from 100 to 300 GPa, this empirical relation would make γ decrease by the same factor over this range at lower temperatures, which is roughly what we see. However, the pressure dependence of γ is very much weakened as T increases, until at 6000 K, γ is almost constant.

2.05.4.2 Elasticity of Solid Iron

A fundamental step toward resolving the structure and composition of the Earth's inner core is to obtain the elastic properties of the candidate phases that could be present.

The elastic constants of h.c.p.-Fe at 39 and 211 GPa have been measured in an experiment reported by Mao *et al.* (1999). Calculations of athermal elastic constants for h.c.p.-Fe have been reported by Stixrude and Cohen (1995b), Söderlind *et al.* (1996), Steinle-Neumann *et al.* (1999), and Vočadlo *et al.* (2003b). These values are presented in Table 2, and plotted as a function of density in Figures 13(a) and 13(b). Although there is some scatter on the reported values of c_{12} , overall the agreement between the experimental and various *ab initio* studies is excellent.

The resulting bulk and shear moduli and the seismic velocities of h.c.p.-Fe as a function of pressure are shown in Figures 14 and 15, along with experimental data. The calculated values compare well with experimental data at higher pressures, but discrepancies at lower pressures are probably due to the neglect of magnetic effects in the simulations (see Steinle-Neumann *et al.*, 1999).

The effect of temperature on the elastic constants of Fe was reported by Steinle-Neumann *et al.* (2001) based on calculations using the approximate 'particle in a cell' method, as discussed in Section 2.05.3. With increasing temperature, they found a significant change in the c/a axial ratio of the h.c.p. structure, which in turn caused a marked reduction in the elastic constants c_{33} , c_{44} , and c_{66} (Figure 16(a)). This led them to conclude that increasing temperature reverses the sense of the single-crystal longitudinal anisotropy of h.c.p.-Fe, and that the anisotropy of the core should now be viewed as being due to h.c.p.-Fe crystals having their c -axis preferably aligned equatorially, rather than axially as originally suggested by Stixrude and Cohen (1995a) (Figures 16(b) and 17).

However, the work of Gannarelli *et al.* (2005) casts doubt on the robustness of the calculations of Steinle-Neumann *et al.* (2001); they found that the c/a ratio ranges from 1.585 at zero pressure and temperature

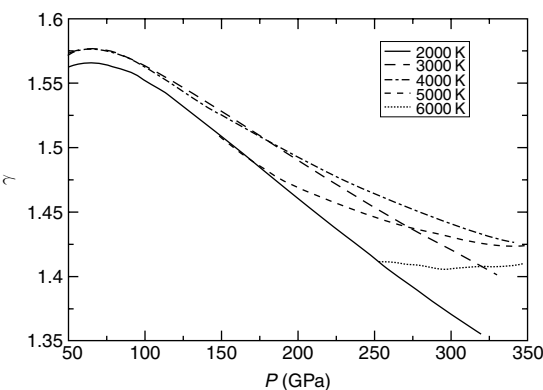


Figure 12 The Grüneisen parameter, γ , as a function of pressure for h.c.p. iron from *ab initio* calculations along isotherms between 2000 and 6000 K (solid lines). From Vočadlo L, Alfe D, Gillan MJ, and Price GD (2003b) The properties of iron under core conditions from first principles calculations. *Physics of the Earth and Planetary Interiors* 140: 101–125.

Table 2 A compilation of elastic constants (c_{ij} , in GPa), bulk (K), and shear (G) moduli (in GPa), and longitudinal (V_p) and transverse (V_s) sound velocity (in km s^{-1}) as a function of density (ρ , in g cm^{-3}) and atomic volume (in \AA^3 per atom)

	V	ρ	c_{11}	c_{12}	c_{13}	c_{33}	c_{44}	c_{66}	K	G	V_p	V_s
Stixrude & Cohen	9.19	10.09	747	301	297	802	215	223	454	224	8.64	4.71
	7.25	12.79	1697	809	757	1799	421	444	1093	449	11.50	5.92
Steinle-Neumann <i>et al.</i>	8.88	10.45	930	320	295	1010	260	305	521	296	9.36	5.32
	7.40	12.54	1675	735	645	1835	415	470	1026	471	11.49	6.13
	6.66	13.93	2320	1140	975	2545	500	590	1485	591	12.77	6.51
Mao <i>et al.</i>	9.59	9.67	500	275	284	491	235	113	353	160	7.65	4.06
	7.36	12.60	1533	846	835	1544	583	344	1071	442	11.48	5.92
Söderlind <i>et al.</i>	9.70	9.56	638	190	218	606	178	224	348	200	8.02	4.57
	7.55	12.29	1510	460	673	1450	414	525	898	448	11.03	6.04
	6.17	15.03	2750	893	1470	2780	767	929	1772	789	13.70	7.24
Vočadlo <i>et al.</i>	9.17	10.12	672	189	264	796	210	242	397	227	8.32	4.74
	8.67	10.70	815	252	341	926	247	282	492	263	8.87	4.96
	8.07	11.49	1082	382	473	1253	309	350	675	333	9.86	5.38
	7.50	12.37	1406	558	647	1588	381	424	900	407	10.80	5.74
	6.97	13.31	1810	767	857	2007	466	522	1177	500	11.77	6.13
	6.40	14.49	2402	1078	1185	2628	580	662	1592	630	12.95	6.59

$K = \langle c_{11} \rangle + 2\langle c_{12} \rangle / 3$ and $G = \langle c_{11} \rangle - \langle c_{12} \rangle + 3\langle c_{44} \rangle / 5$, where $\langle c_{11} \rangle = (c_{11} + c_{22} + c_{33}) / 3$, etc. Previous calculated values are from Stixrude and Cohen (1995b), Steinle-Neumann *et al.* (1999), Söderlind *et al.* (1996), and Vočadlo *et al.* (2003b). The experimental data of Mao *et al.* (1999) are also presented.

to 1.62 at 5500 K and 360 GPa. These lower values for the c/a ratio are confirmed by the work of Vočadlo (2007), who reported elastic constants for both b.c.c.- and h.c.p.-iron using *ab initio* finite temperature molecular dynamics calculations (Table 3).

A further analysis of the high-temperature behavior of iron can be made by considering Birch's law. In the past, Birch's law has been used to make inferences about the elastic properties of the inner core. Birch's law suggests a linear relationship between V_p and ρ , and in the absence of reliable experimental data at very high pressures and temperatures, it has been assumed that this linearity may be extrapolated to the conditions of the inner core. In their very recent work, Badro *et al.* (2006) used inelastic X-ray scattering in a diamond-anvil-cell at high pressures, but ambient temperatures, to demonstrate a linear relationship between V_p and ρ for a number of systems including h.c.p.-Fe. Figure 18 shows the fit to their results extrapolated to core conditions, together with the results from Vočadlo (2007) (where the uncertainties lie within the symbols) and also from shock experiments (Brown and McQueen, 1986). The agreement is generally outstanding; it is noteworthy that the calculated b.c.c.-Fe and h.c.p.-Fe velocity–density systematics are indistinguishable.

Figure 19 shows how V_p varies with density for both athermal and hot *ab initio* calculations (Vočadlo,

2007), together with values from PREM (Dziewonski and Anderson, 1981), experiments of Brown and McQueen (1986) and from a previous computational study (Steinle-Neumann *et al.*, 2001). It is clear that Birch's law holds for the systems studied in the present work, and that the velocities at constant density are almost temperature independent.

The calculated P-wave anisotropy for the h.c.p. and b.c.c. phases of Fe at core conditions is $\sim 6\%$ and $\sim 4\%$, respectively, the former being close to the experimentally determined value of 4–5% (Antonangeli *et al.*, 2004). The seismically observed anisotropy (3–5%; Song and Helberger, 1998) and layering in the inner core could, therefore, be accounted for both phases if the crystals were randomly oriented in the isotropic upper layer and partially aligned in the anisotropic lower layer. In order to make further conclusions about the elasticity of the inner core, the effect of light elements must first be taken into account (see Section 2.05.10).

2.05.5 Rheology of Solid Iron

2.05.5.1 Slip Systems in Iron

In order to understand anisotropy and layering, we need to understand the deformation mechanism and processes which could be responsible for textural

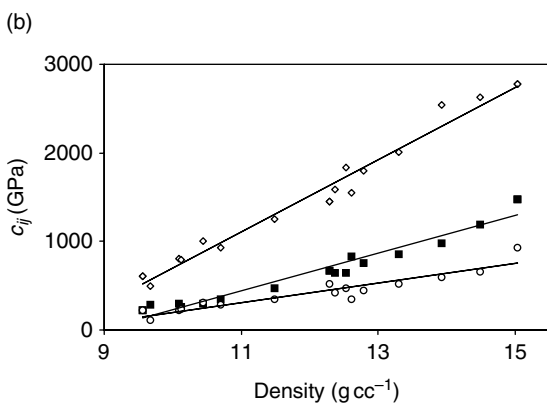
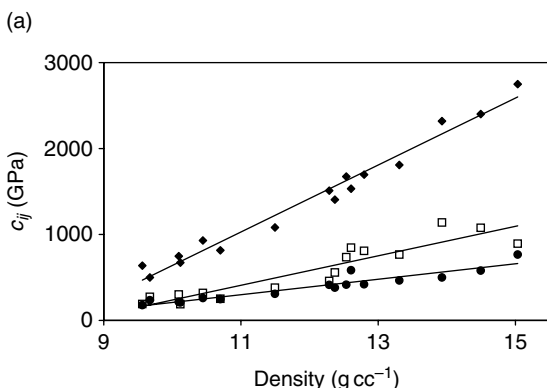


Figure 13 Plot of the elastic constants of h.c.p.-Fe given in Table 2 as a function of density from Stixrude and Cohen (1995b), Söderlind et al. (1996), Steinle-Neumann et al. (1999), and Vočadlo et al. (2003b): (a) c_{11} black diamonds, c_{12} white squares, c_{44} black circles; (b) c_{33} white diamonds, c_{13} black squares and c_{66} white circles.

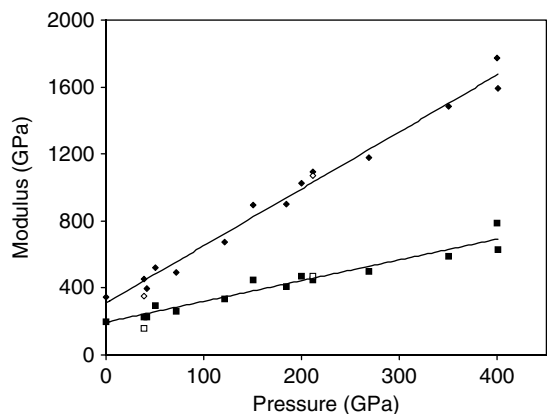


Figure 14 Plot of bulk modulus (diamonds) and shear modulus (squares) for h.c.p.-Fe as a function of pressure, with values taken from Stixrude and Cohen (1995a), Steinle-Neumann et al. (1999), Söderlind et al. (1996), Mao et al. (1999), and Vočadlo et al. (2003b). Black diamonds and squares represent *ab initio* values, while white diamonds and squares represent values obtained from experimentally determined elastic constants.

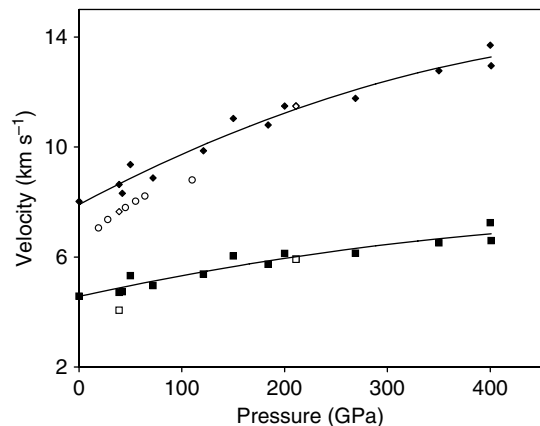


Figure 15 Plot of aggregate V_P (diamonds) and V_S (squares) wave velocity for h.c.p.-Fe as a function of pressure, with values taken from Stixrude and Cohen (1995a), Steinle-Neumann et al. (1999), Söderlind et al. (1996), Mao et al. (1999), and Vočadlo et al. (2003). Black diamonds and squares represent *ab initio* values, while white diamonds and squares represent values obtained from experimentally determined elastic constants. White circles are the experimental data of Fiquet et al. (2001).

development in iron at core conditions. Seismic anisotropy will only be developed during deformation if this deformation leads to lattice-preferred orientation. A dominant slip system may lead to the development of the necessary texture and fabric. It is commonly assumed that glide in crystals occurs along the densest plane of atoms. However, there are exceptions to this rule which prevent this criterion from being predictive, and therefore, in order to determine the favored deformation mechanism in iron, we need to know the primary slip systems in candidate structures under core conditions. Poirier and Price (1999) calculated the elastic constants of h.c.p.-Fe at 0 K together with stacking fault energies for partial dislocations separated by a ribbon of stacking faults lying in the chosen slip plane. They concluded that slip should occur on the basal, rather than prismatic, plane, although it is, however, far from certain that this result will be valid at high temperatures.

If the primary slip system in h.c.p.-Fe becomes prismatic at high temperatures, this will have significant implications for the direction and extent of anisotropy; possible slip systems in h.c.p.-Fe include the basal, prismatic, pyramidal- α and pyramidal- $c+\alpha$ (Merkel et al., 2004). In b.c.c. crystals, primary slip is likely to occur along the plane of the body diagonal because the shortest atomic distance is along $\langle 111 \rangle$. Although the slip direction is always $\langle 111 \rangle$, the slip

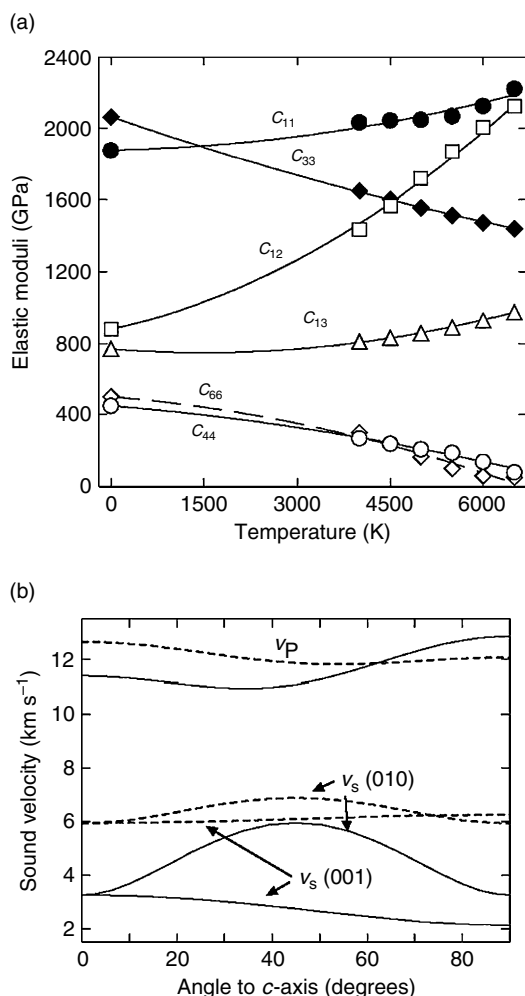


Figure 16 (a) Single-crystal elastic constants as a function of temperature. Note the marked reductions in c_{33} , c_{44} , and c_{66} . (b) Single-crystal velocities in h.c.p.-iron as a function of propagation direction with respect to the c-axis. Results at 6000 K (solid lines) are compared to static results (dashed lines). Note that at 6000 K, $V_P(90^\circ) > V_P(0^\circ)$. After Steinle-Neumann G, Stixrude L, Cohen RE, and Gulseren O (2001) Elasticity of iron at the temperature of the Earth's inner core. *Nature* 413: 57–60.

plane is normally $\{110\}$; however, since the b.c.c. structure is not close packed, other slip planes are possible, namely $\{112\}$ and $\{123\}$. The variety of possible slip systems in b.c.c. metals and the expected modest strain rates in the inner core suggest that b.c.c.-Fe is highly unlikely to develop deformation-driven crystalline alignment. However, very little is known about the dominant slip systems and creep mechanism at core conditions that it is impossible to be definitive.

The existence of a dominant active slip system has consequences for the establishment and magnitude of

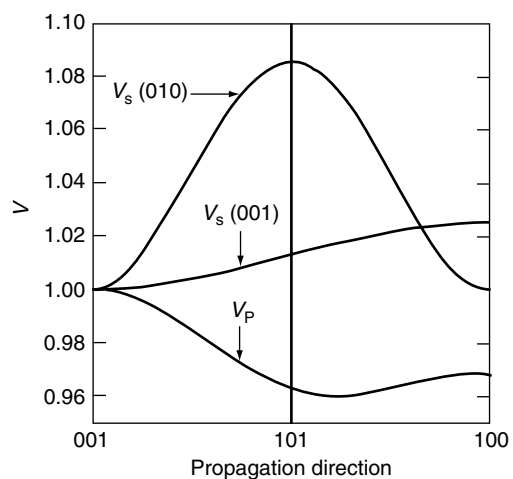


Figure 17 Single-crystal velocities in h.c.p.-iron as a function of propagation direction with respect to the c-axis. Note that $V_P(90^\circ) < V_P(0^\circ)$. After Stixrude L and Cohen RE (1995a) High pressure elasticity of iron and anisotropy of Earth's inner core. *Science* 267: 1972–1975.

anisotropy. If the observed seismic anisotropy in the lower inner core is consistent with that calculated from the elastic constants of high- P/T h.c.p.-Fe phase, and if the h.c.p. phase retains a primary slip system at high P/T leading to preferred orientation, then the anisotropy could have developed either through deformation or on crystallization. If, however, the observed seismic anisotropy in the lower inner core is consistent with that calculated from the elastic constants of the high- P/T b.c.c.-Fe phase, then the anisotropy is most unlikely to be as a result of texture development, but is far more likely to be established on crystallization. However, as we shall see in the next section, recent studies suggest that the inner-core viscosity is low and therefore any textural development on crystallization will have been lost due to the subsequent deformation.

2.05.5.2 Viscosity and the Inner Core

The inner core is not perfectly elastic and has a finite viscosity with deformation occurring over long timescales. Placing numerical constraints on the viscosity of the inner core is fundamental to understanding important core processes such as differential inner-core rotation, inner-core oscillation, and inner-core anisotropy (see Bloxham, 1988).

High-temperature experiments on solid iron at ambient pressure lead to estimates for viscosities of $\sim 10^{13}$ Pa s (Frost and Ashby, 1982); however, this

Table 3 Isothermal (adiabatic) elastic constants and sound velocities of h.c.p.-Fe and b.c.c.-Fe at different densities and temperatures, together with values taken from PREM

	ρ (kg m^{-3})	T (K)	c_{11} (GPa)	c_{12} (GPa)	c_{44} (GPa)	c_{23} (GPa)	c_{33} (GPa)	V_P (km s^{-1})	V_S (km s^{-1})
h.c.p.	11628.1	4000	1129 (1162)	736 (769)	155	625 (658)	1208 (1240)	9.91	4.15
	13155	5500	1631 (1730)	1232 (1311)	159	983 (1074)	1559 (1642)	11.14	4.01
b.c.c.	11592.91	750	1100 (1106)	712 (718)	287			10.11	4.64
	11592.91	1500	1066 (1078)	715 (727)	264			9.98	4.44
	11592.91	2250	1011 (1029)	740 (758)	250			9.88	4.20
	13155	5500	1505 (1603)	1160 (1258)	256			11.29	4.11
	13842	2000	1920 (1967)	1350 (1397)	411			12.22	5.1
	13842	4000	1871 (1966)	1337 (1431)	167			11.66	3.87
	13842	6000	1657 (1795)	1381 (1519)	323			11.83	4.24
PREM	12760							11.02	3.5
	13090							11.26	3.67

Taken from Vočadlo L (2007) *Ab initio* calculations of the elasticity of iron and iron alloys at inner core conditions: evidence for a partially molten inner core? *Earth and Planetary Science Letters*. 254: 227–232.

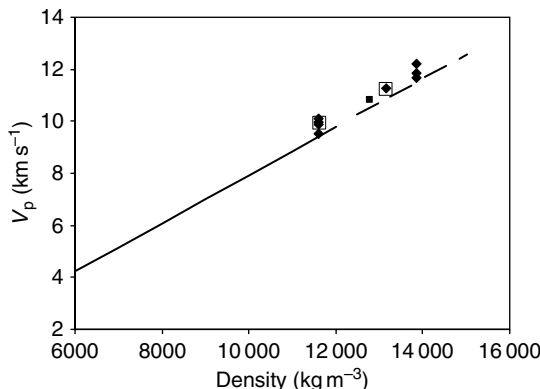


Figure 18 P-wave velocity as a function of density for pure iron compared with the high- P ambient-T DAC experiments of Badro *et al.* (2006); solid line is the fit to data, dashed line is an extrapolation of the fit. Diamonds: calculated b.c.c.-Fe V_P at different temperatures; open squares: calculated h.c.p.-Fe at different temperatures (Vočadlo, 2006); filled square: shock experiments of Brown and McQueen (1986).

is likely to be a lower limit as the value may increase at higher pressures. Seismological and geodetic observations have led to a number of estimates for inner-core viscosity ranging from 10^{11} to 10^{20} Pa s (see Dumberry and Bloxham, 2002). In particular, as we have already seen in Section 2.05.2.3, Buffett (1997) modeled the viscous relaxation of the inner core by calculating the relaxation time for the inner core to adjust, as it rotates, back to its equilibrium shape after small distortions due to perturbations in gravitational potential imposed by the overlying mantle. He suggested that the viscosity has to be constrained to be either less than 10^{16} Pa s (if the whole inner core is involved in

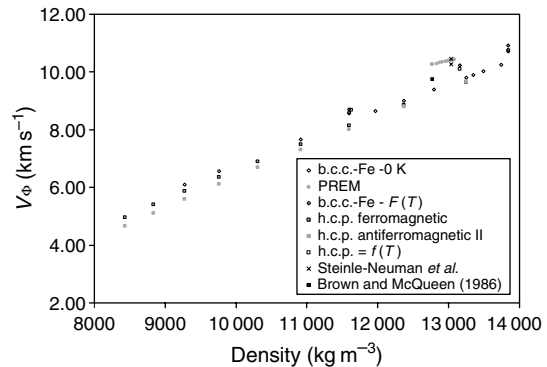


Figure 19 Calculated bulk sound velocity as a function of density for pure iron (Vočadlo, 2006) compared with PREM (Dziewonski and Anderson, 1981), the calculations of Steinle-Neumann *et al.* (2001), and the shock experiments of Brown and McQueen (1986).

the relaxation) or greater than 10^{20} Pa s (if there is no relaxation of the inner core), although the latter case may lead to gravitational locking and hence no differential rotation. In a more recent study, Van Orman (2004) used microphysical models of the flow properties of iron and showed that the dominant deformation process was via Harper-Dorn creep leading to a viscosity of 10^{11} Pa s, at the lowest end of previous estimates. Such a low viscosity would allow the core to adjust its shape and maintain alignment with the mantle on a minute timescale; furthermore, the strain required to produce significant lattice-preferred orientation (LPO) could develop very quickly (years to hundreds of years) suggesting that such deformation could produce the observed anisotropy and all memory if primary crystallization on solidification is lost.

Quantifying the viscosity of the phase(s) present in the inner core at a microscopic level is a very difficult problem. At temperatures close to the melting point (as expected in the inner core), viscous flow is likely to be determined either by dislocation creep (Harper-Dorn creep) or by diffusion creep (Nabarro-Herring creep).

The overall viscosity of inner-core material has diffusion-driven and dislocation-driven contributions:

$$\eta = \left(\left(\frac{1}{\eta_{\text{diff}}} \right) + \left(\frac{1}{\eta_{\text{disl}}} \right) \right)^{-1} \quad [4]$$

Diffusion-controlled viscosity, whereby the material strain is caused by the motion of lattice defects (e.g., vacancies) under applied stress, is given by (Frost and Ashby, 1982)

$$\eta_{\text{diff}} = \frac{d^2 RT}{\alpha D_{\text{sd}} V} \quad [5]$$

where d is the grain size, R is the gas constant, T is the temperature, α is a geometric constant and V is the volume. The self-diffusion coefficient, D_{sd} , is given by (Frost and Ashby, 1982)

$$D_{\text{sd}} = D_0 \exp \left(-\frac{\Delta H}{RT} \right) \quad [6]$$

where D_0 is a pre-exponential factor and ΔH is the activation enthalpy for self-diffusion.

For simple materials, dislocation-controlled viscosity, whereby material strain is caused by the movement of linear defects along crystallographic planes, is given by:

$$\eta_{\text{disl}} = \frac{RT}{\rho D_{\text{sd}} V} \quad [7]$$

where ρ is the dislocation density.

Both dislocation- and diffusion-controlled creep mechanisms are thermally activated and the thermally controlled parameter in both cases is the self-diffusion coefficient, D_{sd} . A commonly used empirical relation for metals assumes that ΔH is linearly proportional to the melting temperature, T_m , and hence that

$$D_{\text{sd}} = D_0 \exp \left(-\frac{g T_m}{T} \right) \quad [8]$$

where g is a constant taking a value of ~ 18 for metals (Poirier, 2002).

Considering iron close to its melting point at core pressures (~ 5500 K), and using reasonable estimates for other quantities ($\alpha \sim 42$, $D_0 \sim 10^{-5} \text{ m}^2 \text{s}^{-1}$, $V \sim 5 \times 10^{-6} \text{ m}^3 \text{ mol}^{-1}$), we obtain values for η_{diff} and η_{disl} of $\sim 10^{21} \text{ d}^2 \text{ Pa s}$ and $\sim 6 \times 10^{22} / \rho \text{ Pa s}$,

respectively. Unfortunately, the strong dependence of the viscosity expressions on the completely unknown quantities of grain size and dislocation density means that it is extremely difficult to produce reliable final numerical values. Grain sizes in the inner core could be anything from 10^{-3} to 10^3 m, resulting in diffusion viscosities in the range $10^{15}\text{--}10^{27}$ Pa s; dislocation densities could be as low as 10^6 m^{-2} or nearer to the dislocation melting limit of 10^{13} m^{-2} , resulting in dislocation-driven viscosities of $10^9\text{--}10^{16}$ Pa s. Thus, even the relative contributions from dislocation-controlled and diffusion-controlled viscosity are as yet unknown.

Clearly, inner-core viscosity is not a well-constrained property, with estimates varying over many orders of magnitude. Future microscopic simulations, combined with high-resolution seismic and geodetic data, should constrain this quantity further and thereby improve our understanding of inner core dynamics.

2.05.6 The Temperature in the Earth's Core

Having shown how mineral physics can be used to understand the properties of solid iron, we turn now to its melting behavior. An accurate knowledge of the melting properties of Fe is particularly important, as the temperature distribution in the core is relatively uncertain and a reliable estimate of the melting temperature of Fe at the pressure of the inner-core boundary (ICB) would put a much-needed constraint on core temperatures. As with the subsolidus behavior of Fe, there is much controversy over its high- P melting behavior (e.g., see Shen and Heinz, 1998). Static compression measurements of the melting temperature, T_m , with the DAC have been made up to ~ 200 GPa (e.g., Boehler, 1993), but even at lower pressures results for T_m disagree by several hundred Kelvin. Shock experiments are at present the only available method to determine melting at higher pressures, but their interpretation is not simple, and there is a scatter of at least 2000 K in the reported T_m of Fe at ICB pressures (see Nguyen and Holmes, 2004).

An alternative to experiment is theoretical calculations which can, in principle, determine accurate melting curves to any desired pressure. Indeed, *ab initio* methods have successfully been used to calculate the melting behavior of transition metals such as aluminum (Vočadlo and Alfè, 2002; **Figure 20**) and copper (Vočadlo *et al.*, 2004). Using the technique of thermodynamic integration, Alfè *et al.* (1999, 2004)

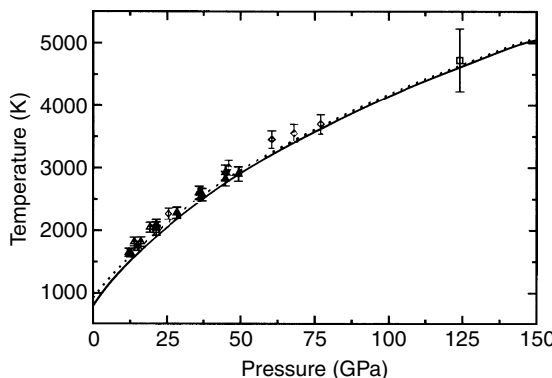


Figure 20 *Ab initio* calculations for the high-pressure melting curve of aluminum (Vočadlo and Alfè, 2002). Solid curve: without pressure correction. Dotted curve: with pressure correction to account for ~2% difference (as a result of using DFT) between calculated and experimental zero pressure equilibrium volume. Diamonds and triangles: DAC measurements of Boehler and Ross (1997) and Hanstrom and Lazor (2000), respectively. Square: shock experiments of Shaner *et al.* (1984).

calculated the melting curve of iron. The condition for two phases to be in thermal equilibrium at a given temperature, T , and pressure, P , is that their Gibbs free energies, $G(P, T)$, are equal. To determine T_m at any pressure, therefore, Alfè *et al.* (2004) calculated G for the solid and liquid phases as a function of T and determined where they are equal. They first calculated the Helmholtz free energy, $F(V, T)$, as a function of volume, V , and hence obtained the pressure through the relation $P = -(\partial F / \partial V)_T$ and G through its definition $G = F + PV$. The free energy of the harmonic solid was calculated using lattice dynamics, while that of the anharmonic solid and the liquid was calculated with molecular dynamics using thermodynamic integration.

Since their first *ab initio* melting curve for Fe was published (Alfè *et al.*, 1999), the authors have improved their description of the *ab initio* free energy of the solid, and have revised their estimate of T_m of Fe at ICB pressures to be ~ 6250 K (see Figure 21 and Alfè *et al.* (2004)), with an error of ± 300 K. For pressures $P < 200$ GPa (the range covered by DAC experiments) their curve lies ~ 900 K above the values of Boehler (1993) and ~ 200 K above the more recent values of Shen *et al.* (1998) (who stress that their values are only a lower bound to T_m). The *ab initio* curve falls significantly below the shock-based estimates for T_m of Yoo *et al.* (1993); the latter deduced the temperature by measuring optical emission (however, the difficulties of obtaining temperature by this method in shock experiments are well known), but accords almost

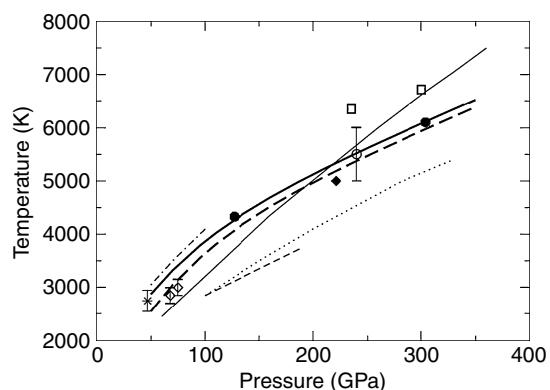


Figure 21 Comparison of the melting curves of Fe from experimental and *ab initio* results from Alfè *et al.* (2004) – heavy solid and long dashed curves: results from Alfè *et al.* (2004) without and with free-energy correction; filled circles: results of Belonoshko *et al.* (2000) corrected for errors in potential fitting; dotted curve: *ab initio* results of Laio *et al.* (2000); light curve: uncorrected *ab initio* results of Belonoshko *et al.* (2000); chained curve and short dashed curve: DAC measurements of Williams *et al.* (1987) and Boehler (1993); open diamonds: DAC measurements of Shen *et al.* (1998); star: DAC measurements of Jephcoat and Besedine (1996); open squares, open circle, and full diamond: shock experiments of Yoo *et al.* (1993), Brown and McQueen (1986), and Nguyen and Holmes (2004).

exactly with the shock data value of Brown and McQueen (1986) and the new data of Nguyen and Holmes (2004). The *ab initio* melting curve of Alfè *et al.* (2004) differs somewhat from the calculations of both Belonoshko *et al.* (2000) and Laio *et al.* (2000). However, the latter two used model potentials fitted to *ab initio* simulations, and so their melting curves are those of the model potential and not the true *ab initio* one (it is important to note here that Laio *et al.* (2000) used a more sophisticated approach in which the model potential had an explicit dependence on thermodynamic state that exactly matched the *ab initio* result). In their paper, Alfè *et al.* (2004) illustrated this ambiguity by correcting for the errors associated with the potential fitting of Belonoshko *et al.* (2000); the result is in almost exact agreement with the true *ab initio* curve (Figure 21). The addition of light elements reduces the melting temperature of pure iron by ~ 700 K making the likely temperature at the inner-core boundary to be ~ 5500 K (Alfè *et al.*, 2002a). An independent measure of the likely temperature in the inner core was made by Steinle-Neumann *et al.* (2001) who performed first-principles calculation of the structure and elasticity of iron at high temperatures; they found that the

temperature for which the elastic moduli best matched those of the inner core was ~ 5700 K.

2.05.7 Thermodynamic Properties of Liquid Iron

The outer core of the Earth is liquid iron alloyed with 5–10% light elements. Experiments on liquid iron at core conditions are prohibitively challenging. However, once more, from the *ab initio* simulation of the free energy of the pure iron liquid, we can obtain first-order estimates for a range of thermodynamic properties at the conditions of the Earth's outer core. Figures 22(a)–22(f) show the results of *ab initio* calculations for values of density, adiabatic and isothermal bulk moduli, thermal expansion coefficient, heat capacity (C_v), Grüneisen parameter and bulk sound velocity, respectively, over a range of pressures and temperatures (see Vočadlo *et al.*, 2003b). Results from the experimental analysis of Anderson and Ahrens (1994) for density and adiabatic incompressibility are also shown (as gray lines; upper: 5000 K, lower: 8000 K). The calculations reproduce the experimentally derived density and incompressibility values to within a few percent. It is worth noting that the bulk sound velocity is almost independent of temperature, confirming the conclusion of Anderson and Ahrens (1994).

2.05.8 Rheology of Liquid Iron

2.05.8.1 Viscosity and Diffusion

Viscosity is a very important parameter in geophysics since the viscosity of materials in the Earth's core are a contributing factor in determining overall properties of the core itself, such as convection and heat transfer; indeed, the fundamental equations governing the dynamics of the outer core and the generation and sustention of the magnetic field are dependent, in part, on the viscosity of the outer core fluid. Quantifying viscosity at core conditions is far from straightforward, especially as the exact composition of the outer core is not known. Furthermore, although there have been many estimates made for outer-core viscosity derived from geodetic, seismological, geomagnetic, experimental, and theoretical studies, the values so obtained span 14 orders of magnitude (see Secco, 1995).

Geodetic observations (e.g., free oscillations, the Chandler wobble, length of day variations, nutation

of the Earth, tidal measurements, and gravimetry) lead to viscosity estimates ranging from 10 mPa s (observations of the Chandler wobble; Verhoogen, 1974) to 10^{13} mPa s (analysis of free oscillation data; Sato and Espinosa, 1967). Theoretical geodetic studies (e.g., viscous coupling of the core and mantle, theory of rotating fluids, inner-core oscillations, and core nutation) lead to viscosity estimates ranging from 10 mPa s (evaluation of decay time of inner-core oscillations; Won and Kuo, 1973) to 10^{14} mPa s (secular deceleration of the core by viscous coupling; Bondi and Lyttleton, 1948). Generally, much higher values for viscosity (10^{10} – 10^{14} mPa s) are obtained from seismological observations of the attenuation of P- and S-waves through the core (e.g., Sato and Espinosa, 1967; Jeffreys, 1959), and from geomagnetic data (e.g., 10^{10} mPa s; Officer, 1986).

The viscosities of core-forming materials may also be determined experimentally in the laboratory and theoretically through computer simulation. Empirically, viscosity follows an Arrhenius relation of the form (see Poirier, 2002)

$$\eta \propto \exp\left(\frac{Q_V}{k_B T}\right) \quad [9]$$

where Q_V is the activation energy. Poirier (1988) analyzed data for a number of liquid metals and found that there is also an empirical relation between Q_V and the melting temperature, consistent with the generalized relationship of Weertman (1970):

$$Q_V \approx 2.6RT_m \quad [10]$$

This very important result implies that the viscosity of liquid metals remains constant (i.e., independent of pressure) along the melting curve and therefore equal to that at the melting point at ambient pressure, which is generally of the order of a few mPa s. Furthermore, Poirier went on to state that the viscosity of liquid iron in the outer core would, therefore, be equal to that at ambient pressure (~ 6 mPa s; Assael *et al.*, 2006).

On a microscopic level, an approximation for the viscosity of liquid metals is given by the Stokes–Einstein equation, which provides a relationship between diffusion and viscosity of the form

$$D\eta = \frac{k_B T}{2\pi a} \quad [11]$$

where a is an atomic diameter, T is the temperature, k_B is the Boltzmann constant, and D is the diffusion coefficient.

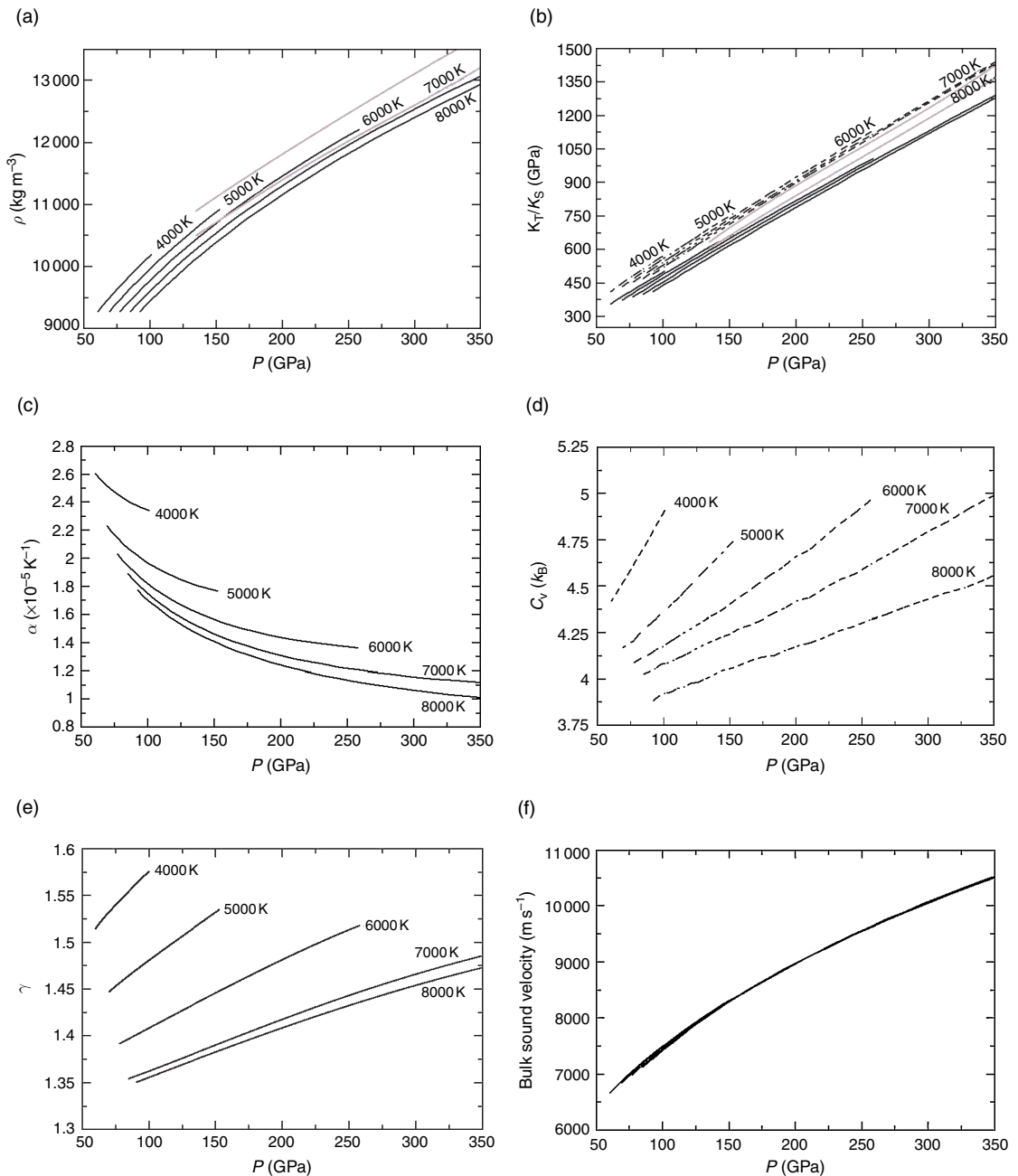


Figure 22 (a–f) Density, incompressibility, thermal expansion, heat capacity, Grüneisen parameter, and bulk sound velocity as a function of pressure for liquid iron. Black lines: *ab initio* calculations (Vočadlo *et al.*, 2003b); gray lines: isentropic model determined from experimental data (upper: 5000 K; lower 8000 K. Anderson and Ahrens (1994)).

Theoretical values for diffusion coefficients have been obtained from *ab initio* molecular dynamics simulations on liquid iron at core conditions, leading to a predicted viscosity of $\sim 12\text{--}15 \text{ mPa s}$ using the Stokes–Einstein relation above. However, although the Stokes–Einstein equation has proved successful in establishing a link between viscosity and diffusion

for a number of monatomic liquids, it is not necessarily the case that it should be effective for alloys or at high pressures and temperatures. More recently, Alfe *et al.* (2000a) used the more rigorous Green-Kubo functions to determine viscosities for a range of thermodynamic states relevant to the Earth's core (Table 4). Throughout this range, the results show

Table 4 The diffusion coefficient D and the viscosity from *ab initio* simulations of ‘liquid iron’ at a range of temperatures and densities (Alfe *et al.*, 2000a)

	$\rho \text{ (kg m}^{-3}\text{)}$					
	9540	10 700	11 010	12 130	13 300	
T (K)	9540	10 700	11 010	12 130	13 300	
$D (10^{-9} \text{ m}^3 \text{ s}^{-1})$	3000 4300 5000 6000 7000	4.0 ± 0.4 5.2 ± 0.2 7.0 ± 0.7 14 ± 1.4 10 ± 1	10 ± 1 13 ± 1.3	9 ± 0.9 11 ± 1.1	6 ± 0.6 9 ± 0.9	5 ± 0.5 6 ± 0.6
$\eta (\text{mPa s})$	3000 4300 5000 6000 7000	6 ± 3 8.5 ± 1 6 ± 3 2.5 ± 2 4.5 ± 2	5 ± 2 7 ± 3	8 ± 3 8 ± 3	15 ± 5 10 ± 3	

that liquid iron has a diffusion coefficient and viscosity similar to that under ambient conditions, a result already suggested much earlier by Poirier (1988). Both *ab initio* calculations and experiments consistently give viscosities of the order of a few mPa s. This suggests that viscosity changes little with homologous temperature, and it is now generally accepted that the viscosity of the outer core is likely to be a few mPa s (comparable to that of water on the Earth’s surface).

2.05.8.2 The Structure of Liquid Iron

It has long been established that liquid structure is approximately constant along the melting curve (e.g., Ross, 1969) and here, in the case of iron, there appears to be a truly remarkable simplicity in the variation of the liquid properties with thermodynamic state; indeed, not only are viscosities and diffusivities almost invariant (as described above), but structural properties show similarly consistent behavior. Alfe *et al.* (2000a) calculated the radial distribution function of liquid iron as a function of temperature at a density of $10\ 700 \text{ kg m}^{-3}$, representative of that in the upper outer core (Figure 23); between 4300 and 8000 K, the effect of varying temperature is clearly not dramatic, and consists only of the expected weakening and broadening of the structure with increasing T .

Furthermore, Shen *et al.* (2004) determined the structure factors of liquid iron as a function of pressure along the melting curve using X-ray scattering in a laser-heated diamond anvil cell up to 58 GPa (Figure 24). Once more, the structure factor preserves

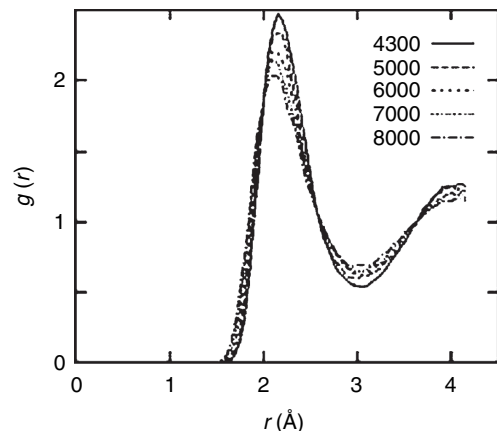


Figure 23 Variation of radial distribution function with temperature from *ab initio* simulations of liquid iron at the fixed density $10\ 700 \text{ kg m}^{-3}$. Adapted from Alfe D, Kresse G, and Gillan MJ (2000a) Structure and dynamics of liquid iron under Earth’s core conditions. *Physics Review B* 61: 132–142.

essentially the same shape; the behavior is consistent with that of close-packed liquid metals. These results provide structural verification of the theoretical predictions given in Figure 23, and also confirm that it is justifiable to extrapolate viscosities measured under ambient conditions to high pressures.

2.05.9 Evolution of the Core

The Earth’s paleomagnetic record suggests that the magnetic field has been operating for over three billion years; the fact that this magnetic field still exists today and has not decayed through Ohmic dissipation (possible on a timescale of $\sim 10^4$ years)

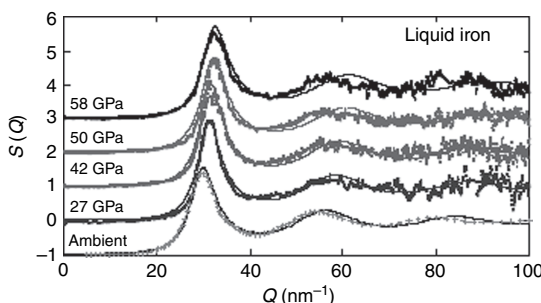


Figure 24 Structure factors of liquid iron along the melting curve determined by X-ray scattering at high pressures (Shen *et al.*, 2004).

suggests that it is being regenerated and sustained by a process such as a geodynamo. For the geodynamo to work, it requires convection of the core fluid (thermal and/or compositional); whether the core is stable to convection depends on the rate of cooling of the core and thus on the evolution of the Earth. As the core cools and solidifies, it releases energy, much of which is transported across the core via conduction. The thermal conductivity of the core material limits the amount of heat which can be transported in this way, and any excess energy may be used to power the geodynamo. The conductivity (both thermal and electrical) of the core material is therefore crucial: if the core material has too high a conductivity, there is no excess heat and therefore no dynamo. A further consideration is the heat flow into the base of the mantle. If this is too large, the core would cool too quickly, and the inner core would grow too rapidly; if the heat flow into the mantle is too low, the core would cool too slowly, convection would be difficult to initiate and sustain, and magnetic field generation would be difficult.

As a result of inner-core growth, the relative contributions of thermal convection to compositional convection have changed over geological time. Thermal convection would have been dominant in the early stages of Earth's evolution, and would have been the sole power source before the formation of the inner core (possibly ~ 2 billion years ago). However, as the inner core grew, compositionally driven convection (from the preferential partitioning of light elements into the outer core and their subsequent buoyancy) became more important (now responsible for $\sim 80\%$ power to geodynamo). Two other important factors which affect the thermal evolution of the core are the possible contribution to

the heat budget from radioactive decay of, for example, ^{40}K , and the ability of the mantle to remove heat away from the core. A reliable thermal evolution model has to reproduce: (1) the correct present-day inner-core size; (2) the present-day heat flux ($\sim 42 \text{ TW}$); (3) the heat flux through the core–mantle boundary (estimates range from 2 to 10 TW); (4) enough entropy to drive a dynamo; and (5) reasonable mantle temperatures.

There have been a number of studies that have developed both analytical and numerical models for the thermal evolution of the core based on calculating heat flux across the core–mantle boundary coupled with heat balance relations associated with core convection and inner-core growth (e.g., Buffett *et al.*, 1992, 1996; Labrosse *et al.*, 2001; Labrosse, 2003; Nakagawa and Tackley, 2004, Gubbins *et al.*, 2003, 2004; Nimmo *et al.*, 2004). The requirement for there to be a radiogenic heat source in order to maintain sufficient power to the geodynamo remains a controversial subject. While some models require a radiogenic heat source, such as potassium, to power the geodynamo (Labrosse, 2003; Nimmo *et al.*, 2004; Costin and Butler, 2006), others suggest that convective processes alone are sufficient to maintain the geodynamo (e.g., Buffett *et al.*, 1996; Christensen and Tilgner, 2004).

However, key to all these thermal evolution models is the need for reliable data for material properties at inner-core conditions. While mineral physics has made some progress (e.g., the quantification of the viscosity of the outer core described in Section 2.05.8.1 and the thermodynamic properties for pure iron described in Sections 2.05.4 and 2.05.7), key properties in the heat transfer relations, such as the electrical and thermal conductivity of iron and iron alloys at core conditions, remain unknown, and are presently only estimated from extrapolations to experimental data.

2.05.10 The Composition of the Core

2.05.10.1 Bulk Composition

The exact composition of the Earth's inner core is not very well known. On the basis of cosmochemical and geochemical arguments, it has been suggested that the core is an iron alloy with possibly as much as ~ 5 wt.% Ni and very small amounts (only fractions of a wt.% to trace) of other siderophile elements such as Cr, Mn, P, and Co (McDonough and Sun, 1995). On the basis of materials-density/sound-wave

velocity systematics, Birch (1964) further concluded that the core is composed of iron that is alloyed with a small fraction of lighter elements. The light alloying elements most commonly suggested include S, O, Si, H, and C, although minor amounts of other elements, such K, could also be present (e.g., Poirier, 1994; Gessmann and Wood, 2002). From seismology it is known that the density jump across the inner-core boundary is between $\sim 4.5\%$ and 6.7% (Shearer and Masters, 1990; Masters and Gubbins, 2003), indicating that there is more light element alloying in the outer core. The evidence thus suggests that the outer core contains $\sim 5\text{--}10\%$ light elements, while the inner core has $\sim 2\text{--}3\%$ light elements. Our present understanding is that the Earth's solid inner core is crystallizing from the outer core as the Earth slowly cools, and the partitioning of the light elements between the solid and liquid is therefore crucial to understanding the evolution and dynamics of the core.

2.05.10.2 The Effect of Nickel

It is generally assumed that the small amount of nickel alloyed to iron in the inner core is unlikely to have any significant effect on core properties as nickel and iron have sufficiently similar densities to be seismically indistinguishable, and addition of small amounts of nickel is unlikely to appreciably change the physical properties of iron. However, very recent *ab initio* calculations at 0 K show that this may not be the case (Vočadlo *et al.*, 2006). The addition of small amounts of nickel (a few atomic percent) by atomic substitution stabilizes the h.c.p. structure with respect to the b.c.c. structure by up to ~ 20 GPa. Experiments at modestly high pressures and temperatures (72 GPa and 3000 K) show that the presence of nickel stabilizes the f.c.c. phase over the h.c.p. phase (Mao *et al.*, 2006). Clearly, full free energy calculations at core temperatures and pressures or further high- P/T experiments are required to resolve this matter. Nevertheless, the previously held assumption that nickel has little or no effect on the first-order elastic properties of iron may not necessarily be valid.

2.05.10.3 Light Elements

In contrast, it has long been known that the presence of light elements in the core does have an effect on core properties. Cosmochemical abundances of the elements, combined with models of the Earth's history,

limit the possible impurities to a few candidates. The light element impurities most often suggested are sulfur, oxygen, and silicon. These alloying systems have been experimentally studied up to pressures of around 100 GPa (e.g., Li and Agee, 2001; Lin *et al.*, 2003; Rubie *et al.*, 2004), and with rapid developments in *in situ* techniques we eagerly anticipate experimental data for iron alloys at the highly elevated pressures and temperatures of the Earth's inner core in the near future. In a study combining thermodynamic modeling with seismology, Helffrich and Kaneshima (2004) modeled the ternary Fe–O–S liquid system at core conditions. It is well known that iron alloy systems exhibit liquid immiscibility, and they wanted to see if such immiscibility could occur in the outer core. If this was the case, layering would occur in the outer core which could be seismologically observable. However, they failed to find any such layering and concluded that, if the outer core was an Fe–S–O alloy, it must exist outside of the two liquid field. This would therefore constrain the composition of the outer core to have < 6 wt.% oxygen and 2–25 wt.% sulfur.

2.05.10.3.1 Chemical potential calculations of FeX binary systems

An alternative approach to understanding the composition of the inner core is to simulate the behavior of these iron alloys with *ab initio* calculations which are readily able to access the pressures and temperatures of the inner core. Alfè *et al.* (2000b, 2002a, 2002b) calculated the chemical potentials of iron in binary systems alloyed with sulfur, oxygen, and silicon. They developed a strategy for constraining both the impurity fractions and the temperature at the ICB based on the supposition that the solid inner core and liquid outer core are in thermodynamic equilibrium at the ICB. For thermodynamic equilibrium the chemical potentials of each species must be equal to both sides of the ICB, which fixes the ratio of the concentrations of the elements in the liquid and in the solid, which in turn fixes the densities. The mole fractions required to reproduce the liquid core density are 16%, 14%, and 18%, respectively, for S, Si, and O (**Figure 25(a)**). If the core consisted of pure iron, equality of the chemical potential (the Gibbs free energy in this case) would tell us only that the temperature at the ICB is equal to the melting temperature of iron at the ICB pressure of 330 GPa. With impurities present, the *ab initio* results reveal a major qualitative difference between oxygen and the other two impurities: oxygen partitions strongly into the liquid, but sulfur and silicon both partition equally in

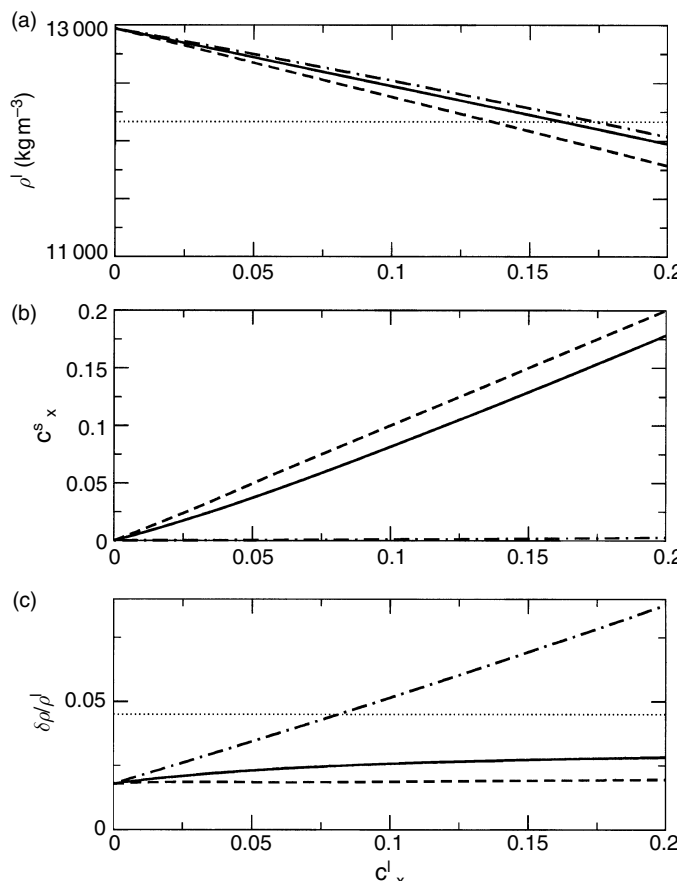


Figure 25 Liquid and solid impurity mole fractions c_x^l and c_x^s of impurities $x = \text{S}, \text{Si}$, and O , and resulting densities of the inner and outer core predicted by *ab initio* simulations. Solid, dashed, and chain curves represent S, Si, and O, respectively. (a) Liquid density ρ^l (kg m^{-3}); horizontal dotted line shows density from seismic data; (b) mole fractions in solid resulting from equality of chemical potentials in solid and liquid; (c) relative density discontinuity ($\delta\rho/\rho$) at the ICB; horizontal dotted line is the value from free oscillation data. Taken from Alfè D, Gillan MJ, Vočadlo L, Brodholt JP, and Price GD (2002b) The *ab initio* simulation of the Earth's Core. *Philosophical Transactions of the Royal Society Series A* 360: 1227–1244.

the solid and liquid. This is shown in Figure 25(b): the calculated chemical potentials in the binary liquid and solid alloys give the mole fractions in the solid that would be in equilibrium with these liquids (i.e., at liquid impurity concentrations corresponding to the seismically observed density in Figure 25(a)) of 14%, 14%, and 0.2%, respectively, for S, Si, and O. Having established the partitioning coefficients, Alfè *et al.* (2000b, 2002a, 2002b) then investigated whether the known densities of the outer and inner core, estimated from seismology, could be matched by one of their calculated binary systems. For sulfur and silicon, their ICB density discontinuities were considerably smaller than the known seismological value at that time of $4.5 \pm 0.5\%$ (Shearer and Masters, 1990); for oxygen, the discontinuity was markedly greater than that from seismology. The

partial volumes in the binary solids give ICB density discontinuities of $2.7 \pm 0.5\%$, $1.8 \pm 0.5\%$, and $7.8 \pm 0.2\%$, respectively (Figure 25(c)). Therefore, none of these binary systems are plausible, that is, the core cannot be made solely of Fe/S, Fe/Si, or Fe/O. However, the seismic data can clearly be matched by a ternary/quaternary system of iron and oxygen together with sulfur and/or silicon. A system consistent with seismic data could contain 8 mol.% oxygen and 10 mol.% sulfur and/or silicon in the outer core, and 0.2 mol.% oxygen and 8.5 mol.% sulfur and/or silicon in the inner core (Alfè *et al.*, 2002a). However, it should be remembered that it is likely that several other light elements could exist in the inner core and would therefore have to be considered before a true description of inner-core composition could be claimed.

2.05.10.3.2 High-temperature elasticity of FeSi and FeS

A fundamental step toward resolving the structure and composition of the Earth's inner core is to obtain the elastic properties of the candidate phases that could be present. Previous work has already suggested that oxygen (see Section 2.05.10.3.1) and carbon (Vočadlo *et al.*, 2002) are unlikely to be the light element in the inner core, while the presence of hydrogen seems questionable as the quantities needed to produce the required density deficit are improbably high (Poirier, 1994), although this certainly cannot be ruled out. Furthermore, experiments (Lin *et al.*, 2002) and theory (Côté *et al.*, 2007) show that the presence of silicon has a significant effect on the phase diagram of iron (Figure 26), significantly stabilizing the b.c.c. phase with respect to the h.c.p. phase.

From experimental and theoretical work, we already know that the shear wave velocities of h.c.p. iron at high pressures are significantly higher than those of the inner core as inferred from seismology (Antonangeli *et al.*, 2004; Mao *et al.*, 2001). We have already seen in Section 2.05.4.2 (Table 3) the elastic properties of pure iron as obtained from *ab initio*

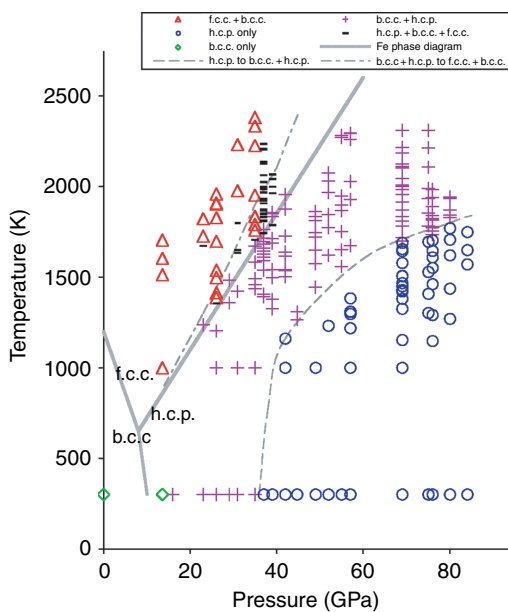


Figure 26 Iron–silicon phases observed in laser-heated diamond anvil cell experiments with the starting materials of Fe (7.9 wt. % Si). The presence of silicon stabilizes the b.c.c. phase with respect to the h.c.p. phase by up to ~40 GPa at high temperatures. After Lin JF, Heinz DL, Campbell AJ, Devine JM, and Shen GY (2002) Iron – Silicon alloy in the Earth's core. *Science* 295: 313–315.

calculations at high temperatures and pressures, and in Table 5 are shown those for FeS and FeSi from Vočadlo (2007). Figure 27 shows the P-wave velocity of FeSi as a function of density compared to the experiments of Badro *et al.* (2006). The agreement is excellent, confirming that this phase too exhibits Birch's law type behavior (see Section 2.05.4.2).

Figure 28 shows how the bulk sound velocity varies for both FeS and FeSi as a function of density for both athermal and hot *ab initio* calculations together with values from PREM (Dziewonski and Anderson, 1981). Once again there seems to be little dependence on temperature of $V_\Phi(\rho)$.

The calculated P-wave anisotropy for both FeS and FeSi is ~6%. The seismically observed anisotropy (3–5%; Song and Helberger, 1998) and layering in the inner core could, therefore, be accounted for by any of the phases studied if the crystals were randomly oriented in the isotropic upper layer and partially aligned in the anisotropic lower layer. However, the fundamental conclusion of these calculations is that, for all candidate core phases, V_S at viable core temperatures (i.e., >5000 K) is more than 10% higher than that inferred from seismology (PREM values between 3.5 and 3.67 km s⁻¹; Dziewonski and Anderson, 1981). Table 3 shows that the calculated values of V_S for pure iron phases are >4.0 km s⁻¹ (in agreement with inferences drawn from the extrapolation of lower pressure experimental data; Antonangeli *et al.* (2004) and also with the value of 4.04 inferred from shock experiments at a density of 12 770 kg m⁻³ (Brown and McQueen, 1986)), while the effect of light elements is to increase the shear wave velocities to over 5 km s⁻¹. If the uncertainties in the seismological values are well constrained, the difference between these observations and the results from both theory and experiment suggests that a simple model for the inner core based on the commonly assumed phases is wrong.

An important consideration is the effect of anelasticity. The reduction in shear wave velocity due to shear wave attenuation is given by

$$V(\omega, T) = V_0(T) \left(1 - \frac{1}{2} \cot\left(\frac{\pi\alpha}{2}\right) Q^{-1}(\omega, T) \right) \quad [12]$$

where $V(\omega, T)$ and $V_0(T)$ are the attenuated and unattenuated shear wave velocities respectively, Q is the quality factor, and α is the frequency dependence of Q . For the inner core $Q = 100$ (Resovsky *et al.*, 2005) and $\alpha = 0.2–0.4$ (Jackson *et al.*, 2000), which result in

Table 5 Isothermal (adiabatic) elastic constants and sound velocities of FeSi and FeS at different densities and temperatures, together with values taken from PREM

ρ (kg m^{-3})	T (K)	c_{11} (GPa)	c_{12} (GPa)	c_{44} (GPa)	c_{23} (GPa)	c_{33} (GPa)	V_P (km s^{-1})	V_S (km s^{-1})
<i>FeSi</i>								
6969.44	1000	488 (489)	213 (214)	125			8.32	4.32
6969.44	2000	425 (428)	238 (241)	150			8.29	4.28
8199.34	1000	938 (942)	413 (417)	263			10.74	5.66
8199.34	2000	863 (871)	431 (439)	263			10.58	5.45
8199.34	3500	788 (803)	469 (484)	250			10.42	5.11
10211.74	5500	1643 (1732)	1030 (1119)	462			13.53	6.26
10402.15	1000	2025 (2043)	1007 (1025)	625			14.34	7.46
10402.15	2000	1909 (1944)	1029 (1064)	583			14.08	7.11
10402.15	3500	1904 (1972)	1117 (1185)	603			14.36	7.06
10402.15	5000	1780 (1874)	1132 (1226)	563			14.12	6.71
<i>FeS</i>								
8587.14	1000	788 (793)	531 (536)	213			10.03	4.56
8587.14	2000	763 (772)	519 (528)	175			9.79	4.23
10353	5500	1294 (1371)	1050 (1127)	257			12.02	4.43
10894.13	1000	1513 (1533)	1400 (1420)	575			13.38	5.81
10894.13	2000	1571 (1613)	1386 (1428)	532			13.43	5.72
10894.13	3500	1545 (1617)	1360 (1432)	492			13.34	5.52
10894.13	5000	1558 (1666)	1379 (1487)	458			13.41	5.34
<i>PREM</i>								
12760							11.02	3.5
13090							11.26	3.67

Taken from Vočadlo L (2007) *Ab initio* calculations of the elasticity of iron and iron alloys at inner core conditions: evidence for a partially molten inner core? *Earth and Planetary Science Letters*. 254: 227–232.

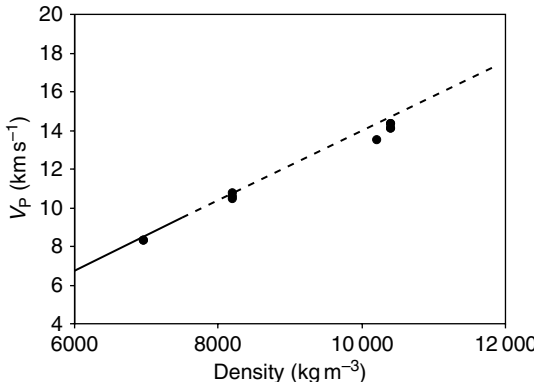


Figure 27 P-wave velocity as a function of density for FeSi compared with the high- P ambient- T DAC experiments of Badro *et al.* (2006); solid line is the fit to data, dashed line is an extrapolation of the fit. Circles: calculated FeSi- V_P at different temperatures (Vočadlo, 2006).

a decrease in the shear velocity of only 0.5–1.5%, nowhere near the >10% difference between the seismological observations and the calculated materials properties. It is important to note that the above analysis is necessarily approximate; anelasticity is a very complex issue that requires material data at the conditions of the Earth's inner core in order to draw

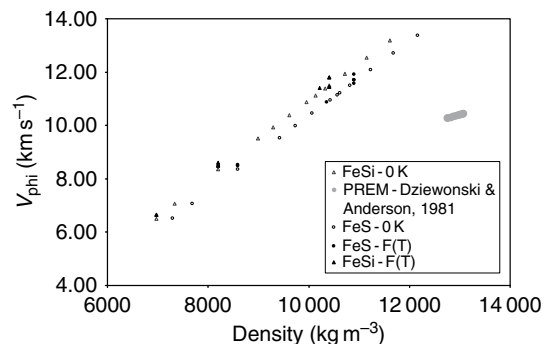


Figure 28 Calculated bulk sound velocity as a function of density for FeS and FeSi (Vočadlo, 2006) compared with PREM (Dziewonski and Anderson, 1981).

irrefutable conclusions – clearly such data are unavailable at present.

Another possible explanation for the difference between the observations and the results from both theory and experiment is that parts of the inner core may be partially molten, with solute rich liquid pockets trapped between solid grains. The amount of melt can be estimated by taking the Hashin–Shtrikman bound for the effective shear modulus of two-phase media leading to a minimum amount of melt in the

inner core is estimated to be $\sim 8\%$. These liquid pockets are not necessarily concentrated in the upper part of the inner core; the observed PKJKP waves go right through the center of the Earth (Cao *et al.*, 2005) so the difference in V_S between seismology (e.g., Dziewonski and Anderson, 1981) and theory suggest that melt may exist throughout the inner core. However, more detailed models involving liquid inclusions can only be tested when more exact, spatially resolved seismological data become available. Whatever the reason for the discrepancy, having shown that attenuation is likely to be small ($\sim 1\%$), the current seismological and standard mineralogical models cannot, at present, be reconciled.

2.05.10.3.3 Rheology of liquid iron alloys

A number of experimental and theoretical studies have been performed on the Fe–FeS system in order to obtain diffusivities and viscosities. High-pressure tracer diffusion experiments (Dobson, 2000) have been carried out on liquid Fe–FeS alloys at 5 GPa resulting in high diffusivities ($10^{-5} \text{ cm}^2 \text{ s}^{-1}$) in excellent agreement with *ab initio* molecular dynamics calculations performed at the same conditions (Vočadlo *et al.*, 2000). When incorporated into the Stokes–Einstein relation (eqn [11]), these diffusivities lead to values for viscosity of a few mPa s, that is, of the same order as that of pure iron.

Direct viscosity measurements (Dobson *et al.*, 2000) of Fe–FeS alloys by means of the falling-sphere technique have been made at similar pressures and temperatures to those used in the diffusion experiments above; these resulted in values for viscosities in excellent agreement with those derived experimentally using the Stokes–Einstein relation. Furthermore, these results are in excellent agreement with *ab initio* molecular dynamics calculations of viscosity based on rigorous Green–Kubo functions of the stresses obtained directly from the simulations (Vočadlo *et al.*, 2000). All of these results thus provide both experimental and theoretical verification of the Stokes–Einstein relation (eqn [11]) and also show that the introduction of light elements into Fe liquid does not appear to significantly affect the values.

Atomistic classical molecular dynamics simulations on the Fe–Ni system (Zhang and Guo, 2000) also show that at the conditions of the Earth's outer core, the viscosities are, again, of the order of that of pure iron indicating that nickel has little or no effect.

2.05.11 Summary

It is clear that mineral physics has a very important role to play in the understanding of the structure, composition, and evolution of the Earth's core. With increasing computer power and the advancing sophistication and precision of experimental techniques, reaching ever high pressures and temperatures, more complex systems will be able to be explored at the conditions of the Earth's core. Results from this research will enable many of the questions concerning the Earth's core to be resolved. The key issues are as follows:

1. Seismological evidence for anisotropy and layering in the inner core is strong, but the mechanism by which this is occurring is unclear at present. With the presence of light elements, it is distinctly possible that the inner-core phase is not just h.c.p.-Fe, but has two or more phases of iron present contributing to the anisotropy and layering. Conversely, both these phenomena could be entirely down to growth mechanisms and therefore only one phase need be present, which, in the presence of light elements, is likely to be b.c.c.-Fe. Full quantification of the thermoelastic properties of multicomponent iron alloy systems at the conditions of the Earth's inner core would enable a compositional model to be developed that is consistent with increasingly accurate seismological data.
2. More precise seismological data, particularly shear wave velocities, along with a better understanding of anelasticity in the inner core, would answer the question as to whether or not there are melt pockets distributed throughout the inner core.
3. Super-rotation of the inner core now seems to be marginal, yet a better understanding of the rheology of the multicomponent systems present would both confirm this and allow an evolutionary model to be developed that is consistent with the present-day Earth.
4. The temperature profile of the core is still unknown; in particular, while the question of the melting temperature of pure iron at inner-core boundary pressures seems to be resolved, it is far from clear exactly what the effect of light elements will be on this quantity.
5. Mineral physics constraints on the thermoelastic properties and processes of multicomponent liquids are essential to both the magnetohydrodynamics relations governing the geodynamo, and also to the core evolution models that determine

the age and heat budget of the Earth; of particular import are better estimates for key parameters for thermal evolution models such as electrical and thermal conductivity.

- Composition models for the outer core can also help clarify the possible structure of the outer core both at the crystallization surface at the inner-core boundary and also in the iron-silicate reaction zone at the core–mantle boundary;

Mineral physics may soon have many of the answers, but results from such advanced theoretical and experimental techniques are nothing without well-constrained seismological data. Models of core composition, structure, and evolution can only be believed when the mineral physics data exactly matches the primary seismological observations. This multidisciplinary approach is the only way forward to a full and thorough understanding of the Earth's core.

References

- Ahrens TJ, Holland KG, and Chen GQ (2002) Phase diagram of iron, revised core temperatures. *Geophysical Research Letters* 29: 1150.
- Alfè D (2005) Melting curve of MgO from first principles simulations. *Physical Review Letters* 94: 235701.
- Alfè D, Gillan MJ, and Price GD (1999) The melting curve of iron at the pressure of the Earth's core from *ab initio* calculations. *Nature* 401: 462–464.
- Alfè D, Gillan MJ, and Price GD (2000b) Constraints on the composition of the Earth's core from *ab initio* calculations. *Nature* 405: 172–175.
- Alfè D, Gillan MJ, and Price GD (2002a) *Ab initio* chemical potentials of solid and liquid solutions and the chemistry of the Earth's core. *Journal Chemical Physics* 116: 7127–7136.
- Alfè D, Gillan MJ, Vočadlo L, Brodholt JP, and Price GD (2002b) The *ab initio* simulation of the Earth's core. *Philosophical Translation of the Royal Society of London Series A* 360: 1227–1244.
- Alfè D, Kresse G, and Gillan MJ (2000a) Structure and dynamics of liquid iron under Earth's core conditions. *Physical Review B* 61: 132–142.
- Alfè D, Price GD, and Gillan MJ (2001) Thermodynamics of hexagonal close-packed iron under Earth's core conditions. *Physical Review B* 64: 045123.
- Alfè D, Vočadlo L, Price GD, and Gillan MJ (2004) Melting curve of materials: theory versus experiment. *Journal of Physics–Condensed Matter* 16: S973–S982.
- Anderson DL (1989) *Theory of the Earth*. Blackwell.
- Anderson OL and Isaak DG (2002) Another look at the core density deficit of Earth's outer core. *Physics of the Earth and Planetary Interiors* 131: 19–27.
- Anderson WW and Ahrens TJ (1994) An equation of state for liquid iron and implications for the Earth's core. *Journal Geophysical Research* 99: 4273–4284.
- Andrault D, Fiquet G, Charpin T, and le Bihan T (2000) Structure analysis and stability field of beta-iron at high P and T. *American Mineralogist* 85: 364–371.
- Andrault D, Fiquet G, Kunz M, Visocekas F, and Hausermann D (1997) The orthorhombic structure of iron: and in situ study at high temperature and high pressure. *Science* 278: 831–834.
- Antonangeli D, Occelli F, and Requardt H (2004) Elastic anisotropy in textured hcp-iron to 112 GPa from sound wave propagation measurements. *Earth and Planetary Science Letter* 225: 243–251.
- Assael MJ, Kakosimos K, Banish RM, et al. (2006) Reference data for the density and viscosity of liquid aluminium and liquid iron. *Journal of Physical and Chemical Reference Data* 35: 285–300.
- Badro J, Fiquet G, Guyot F, et al. (2006) Effect of light elements on the sound velocities in solid iron: Implications for the composition of the Earth's core – Short communication. *Earth and Planetary Science Letters* 254(1–2): 233–238.
- Barron THK (1957) Grüneisen parameters for the equation of state of solids. *Annals of Physics* 1: 77–90.
- Beghein C and Trampert J (2003) Robust normal mode constraints on inner core anisotropy from model space search. *Science* 299: 552–555.
- Belonoshko AB, Ahuja R, and Johansson B (2000) Quasi-*ab initio* molecular dynamics study of Fe melting. *Physical Review Letters* 84: 3638–3641.
- Birch F (1964) Density and composition of the mantle and core. *Journal of Geophysical Research* 69: 4377–4388.
- Bloxham J (1988) Dynamics of angular momentum in the Earth's core. *Annual Reviews in Earth and Planetary Science* 26: 501–517.
- Boehler R (1993) Temperatures in the Earth's core from melting point measurements of iron at high static pressures. *Nature* 363: 534–536.
- Boehler R and Ross M (1997) Melting curve of aluminium in a diamond anvil cell to 0.8 Mbar: implications for iron. *Earth and Planetary Science Letter* 153: 223–227.
- Bondi H and Lyttleton RA (1948) On the dynamical theory of the rotation of the Earth. *Proceedings of the Cambridge Philosophical Society* 44: 345–359.
- Brown JM (2001) The equation of state of iron to 450 GPa: another high pressure phase? *Geophysical Research Letters* 28: 4339–4342.
- Brown JM and McQueen RG (1986) Phase transitions, Grüneisen parameter and elasticity of shocked iron between 77 GPa and 400 GPa. *J. Geophys. Res* 91: 7485–7494.
- Buffett BA (1997) Geodynamic estimates of the viscosity of the inner core. *Nature* 388: 571–573.
- Buffett BA (2002) Estimates of heat flow in the deep mantle based on the power requirements for the geodynamo. *Geophysical Research Letter* 29: 1566.
- Buffett BA, Huppert HE, Lister JR, and Woods AW (1992) Analytical model for the solidification of the Earth's core. *Nature* 356: 329–331.
- Buffett BA, Huppert HE, Lister JR, and Woods AW (1996) On the thermal evolution of the Earth's core. *Journal of Geophysical Research* 101: 7989–8006.
- Buffett BA, Huppert HE, Lister JR, et al. (1992) Analytical model for solidification of the Earth's core. *Nature* 356(6367): 329–331.
- Buffett BA and Wenk HR (2001) Texturing of the Earth's inner core by Maxwell stresses. *Nature* 413: 60–63.
- Cao AM, Romanowicz B, and Takeuchi N (2005) An observation of PKJKP: inferences on inner core shear properties. *Science* 308: 1453–1455.
- Christensen UR and Tilgner A (2004) Power requirement for the geodynamo from ohmic losses in numerical and laboratory dynamics. *Nature* 429: 169–171.
- Collier JD and Helffrich G (2001) Estimate of inner core rotation rate from United Kingdom regional seismic network data and consequences for inner core dynamical behaviour. *Earth and Planetary Science Letter* 193: 523–537.

- Costin SO and Butler SL (2006) Modelling the effects of internal heating in the core and lowermost mantle on the Earth's magnetic history. *Physics of the Earth and Planetary Interiors* 157: 55–71.
- Côté AS, Vočadlo L, and Brodholt J (2007) The effect of silicon impurities on the phase diagram of iron and possible implications for the Earth's core structure (submitted).
- Creager KC (1992) Anisotropy of the inner core from differential travel times of the phases PKP and PKIKP. *Nature* 356: 309–314.
- Creager KC (1997) Inner core rotation rate from small-scale heterogeneity and time-varying travel times. *Science* 278: 1284–1288.
- Dobson DP (2000) Fe-57 and Co tracer diffusion in liquid Fe-FeS at 2 and 5 GPa. *Physics of the Earth and Planetary Interiors* 120: 137–144.
- Dobson DP, Brodholt JP, Vočadlo L, and Chrichton W (2001) Experimental verification of the Stokes-Einstein relation in liquid Fe-FeS at 5 GPa. *Molecular Physics* 99: 773–777.
- Dobson DP, Chrichton WA, Vočadlo L, et al. (2000) *In situ* measurements of viscosity of liquids in the Fe-FeS system at high pressures and temperatures. *American Mineralogist* 85: 1838–1842.
- Duffy TS and Ahrens TJ (1993) Thermal expansion of mantle and core materials at very high pressures. *Geophysical Research Letter* 20: 1103–1106.
- Dumbrerry M and Bloxham J (2002) Inner core tilt and polar motion. *Geophysical Journal International* 151: 377–392.
- Durek JJ and Romanowicz B (1999) Inner core anisotropy by direct inversion of normal mode spectra. *Geophysical Journal International* 139: 599–622.
- Dziewonski AM and Anderson DL (1981) Preliminary reference Earth model. *Physics of the Earth and Planetary Interiors* 25: 297–356.
- Fiquet G, Badro J, Guyot F, Requardt H, and Kirsch M (2001) Sound velocities in iron to 110 gigapascals. *Science* 291: 468–471.
- Frost HJ and Ashby MF (1982) *Deformation Mechanism Maps*. Oxford, UK: Pergamon.
- Gannarelli CMS, Alfè D, and Gillan MJ (2003) The particle-in-a-cell model for *ab initio* thermodynamics: Implications for the elastic anisotropy of the Earth's inner core. *Physics of the Earth and Planetary Interiors* 139: 243–253.
- Gannarelli CMS, Alfè D, and Gillan MJ (2005) The axial ration of hcp iron at the conditions of the Earth's inner core. *Physics of the Earth and Planetary Interior* 152: 67–77.
- Garnero EJ and Jeanloz R (2000) Fuzzy patches on the Earth's core-mantle boundary? *Geophys. Res. Lett* 27: 2777–2780.
- Gessmann CK and Wood BJ (2002) Potassium in the Earth's core? *Earth and Planetary Science Letter* 200: 63–78.
- Grüneisen E (1912) Theorie des festen zuxtandes einatomiger element. *Annals Physik* 12: 257–306.
- Gubbins D, Alfè D, Masters G, Price GD, and Gillan MJ (2003) Can the Earth's dynamo run on heat alone? *Geophysical Journal International* 155: 609–622.
- Gubbins D, Alfè D, Masters G, Price GD, and Gillan MJ (2004) Gross thermodynamics of two-component core convection. *Geophysical Journal International* 157: 1407–1414.
- Gubbins D, Masters TG, and Jacobs JA (1979) Thermal evolution of the Earth's core. *Geophysical Journal of the Royal Astronomical Society* 59: 57–99.
- Hanstrom A and Lazor P (2000) High pressure melting and equation of state of aluminium. *Journal of Alloys and Compounds* 305: 209–215.
- Helffrich G and Kaneshima S (2004) Seismological constraints on core composition from Fe-O-S liquid immiscibility. *Science* 306: 2239–2242.
- Isaak DG and Anderson OL (2003) Thermal expansivity of hcp iron at very high pressure and temperature. *Physica B* 328: 345–354.
- Ishii M and Dziewonski AM (2003) Distinct seismic anisotropy at the centre of the Earth. *Physics of the Earth and Planetary Interiors* 140: 203–217.
- Jackson I, Fitz Gerald JD, and Kokkonen H (2000) High temperature viscoelastic relaxation in iron and its implications for the shear modulus and attenuation of the Earth's inner core. *Journal of Geophysical Research* 105: 23605–23634.
- Jeffreys H (1959) *The Earth, its Origin, History and Physical Constitution*. Cambridge, UK: Cambridge University Press.
- Jephcoat AP and Besedin SP (1996) Temperature measurement and melting determination in the laser heated diamond anvil cell. *Philosophical Transactions of the Royal Society of London* 354: 1333–1390.
- Jephcoat A and Olson P (1987) Is the inner core of the Earth pure iron. *Nature* 325: 332–335.
- Karato S (1993) Inner core anisotropy due to the magnetic field induced preferred orientation of iron. *Science* 262: 1708–1711.
- Kennett BLN, Engdahl ER, and Buland R (1995) Constraints on seismic velocities in the Earth from travel-times. *Geophysical Journal International* 122: 108–124.
- Kennett BLN and Engdahl ER (1991) Travel times for global earthquake location and phase identification. *Geophysical Journal International* 105: 429–465.
- Labrosse S (2003) Thermal and magnetic evolution of the Earth's core. *Physics of the Earth and Planetary Interiors* 140: 127–143.
- Labrosse S, Poirier JP, and Le Mouel JL (2001) The age of the inner core. *Earth and Planetary Science Letters* 190: 111–123.
- Laio A, Bernard S, Chiarotti GL, Scandolo S, and Tosatti E (2000) Physics of iron at Earth's core conditions. *Science* 287: 1027–1030.
- Lei J and Zhao D (2006) Global P-wave tomography: on the effect of various mantle and core phases. *Physics of the Earth and Planetary Interiors* 154: 44–69.
- Li J and Agee CB (2001) Element partitioning constraints on the light element composition of the Earth's core. *Geophysical Research Letters* 28: 81–84.
- Lin JF, Heinz DL, Campbell AJ, Devine JM, and Shen GY (2002) Iron–silicon alloy in the Earth's core? *Science* 295: 313–315.
- Lin JF, Struzhkin VV, Sturhahn W, et al. (2003) Sound velocities of iron-nickel and iron-silicon alloys at high pressures. *Geophysical Research Letters* 30: 2112.
- Ma YZ, Somayazulu M, Shen GY, Mao HK, Shu JF, and Hemley RJ (2004) *In situ* X-ray diffraction studies of iron to Earth core conditions. *Physics of the Earth and Planetary Interiors* 143: 455–467.
- Mao HK, Shu JF, Shen GY, Hemley RJ, Li BS, and Singh AK (1999) Elasticity and rheology of iron above 220 GPa and the nature of the Earth's inner core. *Nature* 396: 741–743 (and correction in *Nature* 399: 280–280.).
- Mao HK, Wu Y, Chen LC, Shu JF, and Jephcoat AP (1990) Static compression of iron to 300 GPa and Fe0.8Ni0.2 alloy to 260 GPa – implications for composition of the core. *Journal of Geophysical Research* 95: 21737–21742.
- Mao WL, Campbell AJ, Heinz DL, and Shen G (2006) Phase relations of Fe-Ni alloys at high pressure and temperature. *Physics of the Earth and Planetary Interiors* 155: 146–151.
- Mao HK, Xu J, Struzhkin VV, et al. (2001) Phonon density of states of iron up to 153 GPa. *Science* 292: 914–916.
- Masters G and Gubbins D (2003) On the resolution of density within the Earth. *Physics of the Earth and Planetary Interiors* 140: 159–167.
- Matsui M and Anderson OL (1997) The case for a body-centred cubic phase (α') for iron at inner core conditions. *Physics of the Earth and Planetary Interiors* 103: 55–62.

- McDonough WF and Sun S-s (1995) The composition of the Earth. *Chemical Geology* 120: 223–253.
- Merkel S, Wenk HR, Gillet P, Mao HK, and Hemley RJ (2004) Deformation of polycrystalline iron up to 30 GPa and 1000 K. *Physics of the Earth and Planetary Interiors* 145: 239–251.
- Nakagawa T and Tackley PJ (2004) Effects of thermo-chemical mantle convection on the thermal evolution of the Earth's core. *Earth and Planetary Science Letter* 220: 107–109.
- Nguyen JH and Holmes NC (2004) Melting of iron at the physical conditions of the Earth's core. *Nature* 427: 339–342.
- Nimmo F, Price GD, Brodholt J, and Gubbins D (2004) The influence of potassium on core and geodynamo evolution. *Geophysical Journal International* 156: 363–376.
- Officer CB (1986) A conceptual model of core dynamics and the Earth's magnetic field. *Journal of Geophysics* 59: 89–97.
- Oreshin SI and Vinnik LP (2004) Heterogeneity and anisotropy of seismic attenuation in the inner core. *Geophysical Research Letters* 31: L02613.
- Ouzounis A and Creager KC (2001) Isotropy overlying anisotropy at the top of the inner core. *Geophysical Research Letter* 28: 4221–4334.
- Poirier JP (1988) Transport properties of liquid metals and viscosity of the Earth's core. *Geophysical Journal International* 92: 99–105.
- Poirier JP (1994) Light elements in the Earth's outer core: a critical review. *Physics of the Earth and Planetary Interiors* 85: 319–337.
- Poirier JP (2000) *Introduction to the Physics of the Earth's Interior*. Cambridge, UK: Cambridge University Press.
- Poirier JP (2002) Rheology: Elasticity and viscosity at high pressure. In: Hemley RJ, Chiariotti GL, Bernasconi M, and Ulivi L (eds.) *Proceedings of the International School of Physics "Enrico Fermi"*, Course CXLVII, Amsterdam: IOS Press.
- Poirier JP and Price GD (1999) Primary slip system of epsilon iron and anisotropy of the Earth's inner core. *Physics of the Earth and Planetary Interiors* 110: 147–156.
- Poupinet G, Souriau A, and Coutant O (2000) The existence of an inner core super-rotation questioned by teleseismic doublets. *Physics of the Earth and Planetary Interiors* 118: 77–88.
- Resovsky J, Trampert J, and Van der Hilst RD (2005) Error bars in the global seismic Q profile. *Earth and Planetary Science Letter* 230: 413–423.
- Romanowicz B (2003) Global mantle tomography: progress status in the past 10 years. *Annual Review Earth and Planetary Science* 31: 303–328.
- Ross M (1969) Generalised Lindemann melting law. *Physical Review* 184: 233–242.
- Rost S and Revenaugh J (2001) Seismic detection of rigid zones at the top of the core. *Science* 294: 1911–1914.
- Rubie DC, Gessmann CK, and Frost DJ (2004) Partitioning of oxygen during core formation of the Earth and Mars. *Nature* 429: 58–61.
- Sato R and Espinosa AF (1967) Dissipation factor of the torsional mode ωT_2 for a homogeneous mantle Earth with a soft-solid or viscous-liquid core. *Journal of Geophysical Research* 72: 1761–1767.
- Saxena SK and Dubrovinsky LS (2000) Iron phases at high pressures and temperatures: Phase transitions and melting. *American Mineralogist* 85: 372–375.
- Saxena SK, Dubrovinsky LS, and Haggkvist P (1996) X-ray evidence for the new phase of beta-iron at high temperature and high pressure. *Geophysical Research Letter* 23: 2441–2444.
- Secco RA (1995) Viscosity of the outer core. In: Ahrens TJ (ed.) *Mineral Physics and Crystallography: A Handbook of Physical Constants*, AGU Reference Shelf 2, pp. 218–226. Washington: AGU.
- Shaner JW, Brown JM, and McQueen RG (1984) In: *High Pressure in Science and Technology*, Homan C, Mac-Crone RK, and Whalley E (eds.) p. 137. Amsterdam: North Holland.
- Shearer P and Masters G (1990) The density and shear velocity contrast at the inner core boundary. *Geophysical Journal International* 102: 491–498.
- Shen GY and Heinz DL (1998) High pressure melting of deep mantle and core materials. *Reviews in Mineralogy* 37: 369–396.
- Shen GY, Mao HK, Hemley RJ, Duffy TS, and Rivers ML (1998) Melting and crystal structure of iron at high pressures and temperatures. *Geophysical Research Letters* 25: 373–376.
- Shen GY, Prakapenka VB, Rivers ML, and Sutton SL (2004) Structure of liquid iron at pressures up to 58 GPa. *Physical Review Letters* 92: 185701.
- Shimizu H, Poirier JP, and Le Mouel JL (2005) On the crystallisation at the inner core boundary. *Physics of the Earth and Planetary Interiors* 151: 37–51.
- Söderlind P, Moriarty JA, and Wills JM (1996) First principles theory of iron up to earth's core pressures: structural, vibrational and elastic properties. *Physical Review B* 53: 14063–14072.
- Soldati G, Boschi L, and Piersanti A (2003) Outer core density heterogeneity and the discrepancy between PKP and PcP travel time observations. *Geophysical Research Letter* 30: 1190.
- Song X (1997) Anisotropy of the Earth's inner core. *Reviews of Geophysics* 35: 297–313.
- Song XD (2000) Joint inversion for inner core rotation, inner core anisotropy and mantle heterogeneity. *Journal of Geophysical Research* 105: 7931–7943.
- Song XD and Helmberger DV (1993) Anisotropy of Earth's inner core. *Geophysical Research Letter* 20: 2591–2594.
- Song XD and Helmberger DV (1998) Seismic evidence for an inner core transition zone. *Science* 282: 924–927.
- Song XD and Li AY (2000) Support for differential inner core superrotation from earthquakes in Alaska recorded at South Pole station. *Journal of Geophysical Research* 105: 623–630.
- Song XD and Richards PG (1996) Seismological evidence for differential rotation of the Earth's inner core. *Nature* 382: 221–224.
- Song XD and Xu XX (2002) Inner core transition zone and anomalous PKP(DF) waveforms from polar paths. *Geophysical Research Letters* 29: 1042.
- Souriau A (1998) New seismological constraints on differential rotation of the inner core from Novaya Zemlya events recorded at DRV, Antarctica. *Geophysical Journal International* 134: F1–F5.
- Steinle-Neumann G, Stixrude L, and Cohen RE (1999) First principles elastic constants for the hcp transition metals Fe, Co and Re at high pressure. *Physical Review B* 60: 791–799.
- Steinle-Neumann G, Stixrude L, Cohen RE, and Gulseren O (2001) Elasticity of iron at the temperature of the Earth's inner core. *Nature* 413: 57–60.
- Steinle-Neumann G, Stixrude L, and Cohen RE (2002) Physical properties of iron in the inner core. In: Dehant V, Creager K, Zatman S, and Karato S-I (eds.) *Core Structure, Dynamics and Rotation*, pp. 137–161. Washington, DC: AGU.
- Stixrude L and Brown JM (1998) The Earth's core. *Review in Mineralogy* 37: 261–282.
- Stixrude L and Cohen RE (1995a) High pressure elasticity of iron and anisotropy of Earth's inner core. *Science* 267: 1972–1975.
- Stixrude L and Cohen RE (1995b) Constraints on the crystalline structure of the inner core – mechanical stability of bcc iron at high pressure. *Geophysical Research Letters* 22: 125–128.
- Stixrude L, Wasserman E, and Cohen RE (1997) Composition and temperature of the Earth's inner core. *Journal of Geophysical Research* 102: 24729–24739.

- Su WJ, Dziewonski AM, and Jeanloz R (1996) Planet within a planet: rotation of the inner core of the Earth. *Science* 274: 1883–1887.
- Sun XL and Song XD (2002) PKP travel times at near antipodal distances: implications for inner core anisotropy and lowermost mantle structure. *Earth and Planetary Science Letters* 199: 429–445.
- Van Orman JA (2004) On the viscosity and creep mechanism of Earth's inner core. *Geophysical Research Letter* 31: L20606.
- Verhoogen J (1974) Chandler wobble and viscosity in the Earth's core. *Nature* 249: 334–335.
- Vočadlo L (2007) *Ab initio* calculations of the elasticity of iron and iron alloys at inner core conditions: evidence for a partially molten inner core? *Earth and Planetary Science Letters* 254: 227–232.
- Vočadlo L and Alfe D (2002) *Ab initio* melting curve of the fcc phase of aluminium. *Physical Review B* 65: 214105: 1–12.
- Vočadlo L, Alfe D, Gillan MJ, Wood IG, Brodholt JP, and Price GD (2003a) Possible thermal and chemical stabilisation of body-centred-cubic iron in the Earth's core. *Nature* 424: 536–539.
- Vočadlo L, Alfe D, Gillan MJ, and Price GD (2003b) The properties of iron under core conditions from first principles calculations. *Physics of the Earth and Planetary Interiors* 140: 101–125.
- Vočadlo L, Alfe D, Price GD, and Gillan MJ (2004) *Ab initio* melting curve of copper by the phase coexistence approach. *Journal of Chemical Physics* 120: 2872–2878.
- Vočadlo L, Brodholt JP, Alfe D, Gillan MJ, and Price GD (2000) *Ab initio* free energy calculations on the polymorphs of iron at core conditions. *Physics of the Earth and Planetary Interiors* 117: 123–137.
- Vočadlo L, Brodholt J, Dobson D, Knight KS, Marshal WG, Price GD, and Wood IG (2002) The effect of ferromagnetism on the equation of state of Fe3C studied by first principles calculations. *Earth and Planetary Science Letters* 203: 567–575.
- Vočadlo L, Dobson DP, and Wood IG (2006) An *ab initio* study of nickel substitution into iron. *Earth and Planetary Science Letters* 248: 132–137.
- Weertman J (1970) The creep strength of the Earth's mantle. *Reviews of the Geophysics and Space Physics* 8: 145–168.
- Williams Q, Jeanloz R, Bass J, Svendsen B, and Ahrens TJ (1987) The melting curve of iron to 250 Gigapascals: a constraint on the temperature at the Earth's centre. *Science* 236: 181–182.
- Won IJ and Kuo JT (1973) Oscillation of the Earth's inner core and its relation to the generation of geomagnetic field. *Journal of Geophysical Research* 78: 905–911.
- Yoo CS, Holmes NC, Ross M, Webb DJ, and Pike C (1993) Shock temperature and melting of iron at Earth's core conditions. *Phys. Rev. Lett* 70: 3931–3934.
- Yoshida S, Sumita I, and Kumazawa M (1996) Growth model of the inner core coupled with the outer core dynamics and the resulting anisotropy. *Journal of Geophysical Research* 101: 28085–28103.
- Zhang YG and Guo Gj (2000) Molecular dynamics calculation of the bulk viscosity of liquid iron-nickel alloy and the mechanism for the bulk attenuation of seismic waves in the Earth's outer core. *Physics of the Earth and Planetary Interiors* 122: 289–298.
- Zhang J, Song XD, Li YC, et al. (2005) Inner core differential motion confirmed by earthquake waveform doublets. *Science* 309(5739): 1357–1360.